1-1-2013

Pu-based solutions for slope stabilizing piles

Wei Dong Guo
University of Wollongong, wdguo@uow.edu.au

Pu-based solutions for slope stabilizing piles

Abstract

This paper proposes an equivalent load transfer approach for simulating the response of passive piles owing to soil movement. The approach is elaborated for two commonly seen (normal and deep) sliding modes. In terms of compatibility conditions across sliding and stable layers, new coupled elastic (sliding layer)-elastic (stable layer) (E-E) solutions, and plastic (sliding layer)-elastic-plastic (stable layer) (P-EP) solutions are developed. The solutions are implemented into a program called GASMove operating in the mathematical software Mathcad. They are compared with available numerical analyses, and employed to the predict response of eight instrumented piles. The study reveals the proposed equivalent load-soil movement relationship works well along with the solutions; the E-E solution generally offers good prediction for piles with infinite lengths in both sliding and stable layers (deep sliding mode); the P-EP solution is good for piles rotating rigidly in a sliding layer (normal sliding mode); and similar predictions may be gained from different sets of p(u) and k profiles, as with laterally loaded piles, but a linear p(u) should be used for the stable layer to gain the smallest pile resistance. Design charts are generated to facilitate the prediction of a nonlinear response of passive piles, for which example predictions are elaborated. (C) 2013 American Society of Civil Engineers.

Keywords

pu, slope, stabilizing, piles, solutions

Disciplines

Engineering | Science and Technology Studies

Publication Details

Guo, W. Dong. (2013). Pu-based solutions for slope stabilizing piles. International Journal of Geomechanics, 13 (3), 292-310.

P_U BASED SOLUTIONS FOR SLOPE STABILISING PILES

Wei Dong Guo [1]

ABSTRACT

This paper proposes an equivalent load transfer approach for simulating response of passive piles owing to soil movement. The approach is elaborated for two commonly seen (normal and deep) sliding modes. In terms of compatibility conditions across sliding and stable layers, new coupled elastic (sliding layer) –elastic (stable layer) (i.e. E-E) solutions, and plastic (sliding layer) - elastic-plastic (stable layer) (i.e. P-EP) solutions are developed. The solutions are implemented into a program called GASMove operating in the mathematical software Mathcad™. They are compared with available numerical analyses, and employed to predict response of eight instrumented piles.

The study reveals (1) The proposed equivalent load~soil movement relationship works well along with the solutions; (2) The E-E solution generally offers good prediction for piles with infinite lengths in both sliding and stable layers (deep sliding mode). (3) The P-EP solution is good for piles rotating rigidly in sliding layer (normal sliding mode); and (4) Similar predictions may be gained from different sets of p_u and k profiles, as with laterally loaded piles, but a linear p_u should be used for stable layer to gain smallest pile resistance.

Design charts are generated, to facilitate prediction of nonlinear response of passive piles, for which example predictions are elaborated.

Key words: passive piles; closed form solutions; soil movement; pile-slope interaction

---

Associate Professor, School of Civil, Mining and Environmental Engineering, University of Wollongong NSW, 2522, Australia, Tel.: 612- 42213036,**wdguo@uow.edu.au**

INTRODUCTION

Passive piles refer to those piles subjected to soil movement, as commonly seen in stabilising a sliding slope (Viggiani 1981) (see Fig. 1a), and supporting bridge abutments (Springman 1989; Stewart et al. 1994). Laterally loaded (i.e. active) piles may act as passive ones once subjected to the driving action of adjacent piles (Henke 2009), or nearby excavation activity (Chen and Poulos 1997; Leung et al. 2000; Choy et al. 2007). Predicting the response of passive piles by and large has recourse to numerical solutions (Byrne et al. 1984; Chen and Poulos 1997; Chen and Martin 2002; Mostafa and Naggar 2006). The solutions are powerful and useful, but would not warrant consistency in predictions (Poulos 1995; Chow 1996; Potts 2003). In particular, they are generally based on a uniform limiting force profile, which is not observed along test piles (Matlock 1970; Yang and Jeremic 2002; Guo 2006).

Figure 1a shows a passive pile in an unstable slope to be addressed herein. Subjected to a lateral uniform soil movement w_s, the pile has an embedded length L_i in i^{th} layer. Note subscript i = 1, and 2 denote the sliding and stable layer, respectively in this paper. The impact of the movement w_s on the pile is encapsulated into an equivalent load (thrust) H_2. By incorporating boundary conditions, behaviour of the pile may be modelled by using the solution for an active pile under the load H_2 at an eccentricity e_{o2} (see Fig. 1c), for the stable layer, or under H_1 (=-H_2) for the sliding layer (Fig. 1d and e). The use of the concentrated force H_i at sliding depth to model the pile response is sufficiently accurate (Fukuoka 1977). The thrust H_2 and the eccentricity e_{o2} (= -e_{o1}) above the point O at sliding level (Fig. 1c) causes a dragging moment M_{o2} (= H_2e_{o2}) above the point, and M_{o1} = M_{o2}. Note the H_2 is the horizontal component of net sliding force (thrust) along the

oblique sliding interface. A high eccentricity e_{o2} (thus M_{o2}) leads to a low shear force and deflection (Matlock et al. 1980; Guo 2009) at the point O, which need to be determined.

Design of passive piles generally requires the maximum shear force H_2 or H_1 in each pile (Poulos 1995; Guo and Qin 2010), and the dragging moment M_{o2}, which in turn are dominated by the limiting force per unit length p_{ui} and the depth of its mobilisation x_{pi} between the pile and the soil. The p_{ui} profile, stipulated the same as that for an active pile (Chen et al. 2002), significantly overestimates the resistance on piles adjacent to excavation (Leung et al. 2000).

Four pile-soil interaction modes have been revealed to date, for which analytical solutions are established.

- Plastic flow mode: Soil flows around a stationary pile, on which ultimate pressure can be estimated using plasticity theory (Ito and Matsui 1975; De Beer and Carpentier 1977).
- Rigid pile mode: A rigid pile rotates with sliding clay, for which maximum shear forces and bending moments are obtained assuming uniform resistances along the pile in sliding and stable clay layers (Viggiani 1981; Chmoulian 2004; Smethurst and Powrie 2007; Frank and Pouget 2008).
- Normal and deep sliding modes: A pile rotates rigidly only in the sliding layer (normal sliding mode, see Fig. 1d), or with infinite lengths in either layer, a pile deforms flexibly and moves with sliding soil (deep sliding mode, Fig. 1e). Elastic solutions are proposed for gaining profiles of bending moment, deflection and shear force, in light of a measured sliding force H (= H_1, Fig. 1d), and a measured differential angle θ_o at the point O between the slope angles θ_{g1} and θ_{g2} of the pile in sliding and stable layers, respectively (see Fig. 1d and e). Note the angle θ_o is equal

to $-\theta_{g2}-\theta_{g1}$, with $\theta_{g1}>0$, and $\theta_{g2}<0$. It is negligibly small for a uniform soil movement (Fukuoka 1977) associated with a deep sliding mode; or it is approximately equal to the gradient of a linear soil movement with depth (Cai and Ugai 2003) concerning the normal sliding mode. The H_2 was linked to soil movement w_s. With H_2 from w_s, elastic-plastic solutions for a laterally loaded pile (Fig. 1b) are used to model passive piles without dragging (i.e. zero bending moment at the sliding level) (Guo 2003).

The aforementioned solutions were generally validated using pertinent instrumented pile response, but are unable to capture the coupled impact of soil movement and any non-zero dragging moment (dragging case) on the piles. The objectives of this study are

- To develop a new E-E(coupled) solution to model deep sliding case, in which two 'E' refer to 'elastic' pile-soil interaction in sliding and stable layer, respectively, and 'coupled' interaction among different layers is incorporated.
- To deduce a practical P-EP solution to capture impact of dragging, and rigid rotation, for which a plastic (P) pile-soil interaction is stipulated in sliding layer, and elastic-plastic (EP) interaction in stable layer; and
- To establish sliding force (H) and soil movement (w_s) correlations for the normal and deep sliding modes, respectively.

The solutions are entered into programs operating in Mathcad^{TM} (www.PTC.com) and EXCEL^{TM}. They are compared with boundary element analysis (BEA), and used to study eight instrumented piles to unlock any salient features of the passive piles. The P-EP solution is employed to develop design charts, and their use is illustrated via a typical example.

ELASTIC-PLASTIC (EP) SOLUTION

Load Transfer model

An elastic-plastic (EP) solution for an infinitely long, active pile (Guo 2006) (in Fig. 1c) was developed, in light of a load transfer model, in which the pile-soil interaction is modelled by a series of springs distributed along the shaft.

- Each spring is described by an ideal elastic-plastic p_i-y_i (w_i) curve, which has a gradient (i.e. modulus of subgrade reaction), k_i, and a net ultimate lateral resistance per unit pile length p_{ui}. Note the p_i and $y_i(w_i)$ are the local net force per unit length, and pile deflection respectively.
- The coupled effect among the springs is captured by a fictitious tension membrane (N_{pi}) in the elastic zone, and it is neglected in the plastic zone.

The EP solution is dominated by the critical parameters k_i, N_{pi} and p_{ui}, which are calculated from two input parameters G_{si}, and A_{Li}.

(1) Values of k_i/G_{si} and $4N_{pi}/(\pi d^2 G_{si})$ are correlated to pile slenderness ratio L_i/d, loading eccentricity e_{oi}, and pile-soil relative stiffness E_p/G_{si} (L_i = pile lengths in i^{th} layer; d and E_p = diameter and Young's modulus of an equivalent solid pile, respectively; and G_{si} = soil shear modulus).

(2) Ignoring sliding resistance at sliding surface, the net limiting force on a unit length p_{ui} varies with depth and is given by (Guo 2003; Guo 2006)

$$p_{ui} = A_{Li} x_i^{n_i} \tag{1}$$

where x_i = depth measured from point O; n_i = power to the equivalent depth of x_i; and A_{Li} = gradient of the p_{ui} profile with depth (see Table 1). Over the thickness of the plastic zone, x_{pi} from the point O, the net mobilized p_i attains the p_{ui}, otherwise, beyond the x_{pi}, it is proportional to pile deflection w_i. Especially, the p_{ui} for layered soils must satisfy Eq.

(1) within the maximum x_{pi} (induced by maximum load H_2) and $p_{ui} \leq 11.9d(\max s_{ui})$ (Note max s_{ui} = maximum s_{ui}) (Randolph and Houlsby 1984).

The EP solution capitalised on a constant k_i and the aforementioned p_{ui} is indeed sufficiently accurate for modelling active piles (Murff and Hamilton 1993; Guo 2006) compared to numerical approaches (Yang and Jeremic 2002; Guo 2009). It is also useful for calibrating pertinent numerical results (Guo 2010). It is thus used here to model passive piles in stable layer. The values of the parameters A_{Li}, n_i and G_{si} for active piles (see Table 1) are generally valid for passive piles (Guo and Ghee 2004; Guo and Qin 2010), but for (1) a much lower p_{ui} on piles adjacent to excavation (Leung et al. 2000; Chen et al. 2002); and (2) An increased critical length of $1.2L_{c1}+x_{p1}$ in the sliding layer (in which L_{c1} = the critical length of an active pile in sliding layer), owing to dragging eccentricity e_{o2}. The thrust H is determined next.

EQUIVALENT LOAD (THRUST) FOR PASSIVE PILES

The thrust H ($=H_1=-H_2$) (see Fig. 1d) and moment induce a rotation angle θ_{gi}, and a lateral pile deflection w_{gi} at the point O, which are geometrically related to the uniform soil movement w_s (see Fig. 1d and e, and Table 2) by

$$w_s = w_{g1} + w_{g2} + \theta_o (L_1 - x_s) \tag{2}$$

where x_s = thickness of the resistance zone, in which the pile deflection exceeds the soil movement w_s. Eq. (2) is valid, so long as $x_s \leq L_1 \leq 1.2L_{c1}+x_{p1}$ or $w_{g2}+|\theta_{g2}| L_1 > w_s > w_{g2}$; Otherwise, a w_s higher than pile movement would render 'plastic flow mode' to occur. As shown in Fig. 1(d), the rotation causes the rigid movement $\theta_o(L_1-x_s)$ over the thickness of L_1-x_s, which becomes negligible ($\theta_o \approx 0$) for deep sliding case. Use of Eq. (2) is elaborated next for the two sliding modes.

Normal Sliding

A normal sliding mode (see Fig. 1d) is anticipated, once $L_1 \le 1.2L_{c1}+x_{p1}$. This mode is characterised by rigid rotation of the pile about the point O (i.e. $w_{g1} \approx 0$, $\theta_{g1} \approx 0$, and $\theta_o = -\theta_{g2}$) in the sliding layer, but infinitely long in the stable layer. The total pile movement is equal to: (1) w_{g2} at sliding level (i.e. $x_s = L_1$), and (2) $w_{g2}+|\theta_{g2}|L_1$ at ground level ($x_s = 0$), respectively.

Assuming a plastic pile-soil interaction in sliding layer, the sliding force per unit length p_{u1} is stipulated as $A_{L1}\xi$ in the resistance zone of $x = 0 \sim x_s$, and as A_{L1} in the thrust zone of $x = x_s \sim L_1$, respectively (see Fig.1b and d). The factor ξ is used to capture the combined impact of pile-head constraints and soil resistance. Integrating the p_{u1} over the sliding depth offers

$$H_1 = A_{L1}[L_1 - (1+\xi)x_s] \tag{3}$$

Eq. (2) offers $L_1 - x_s = [w_s - (w_{g1} + w_{g2})]/\theta_o$, which allows H_1 of Eq. (3) to be recast into

$$H_1 = (1+\xi)A_{L1}\frac{w_s - w_{g2}}{|\theta_{g2}|} + \xi A_{L1}L_1 \tag{4}$$

where w_{g2} and θ_{g2} may be determined using the normalised $\overline{w}_{g2}$ and $\overline{\theta}_{g2}$ from elastic-plastic solutions of an infinitely long pile in stable layer (Guo 2006).

$$\begin{aligned}\overline{w}_{g2} = \frac{w_{g2}k_2\lambda_2^{n_2}}{A_{L2}} = \frac{2}{3}\bar{x}_{p2}^{n_2+3}\frac{2\bar{x}_{p2}^2 + (2n_2+10)\bar{x}_{p2} + n_2^2 + 9n_2 + 20}{(\bar{x}_{pi}+1)(n_2+2)(n_2+4)} \\ + \frac{(2\bar{x}_{p2}^2 + 2\bar{x}_{p2} + 1)\bar{x}_{p2}^{n_2}}{\bar{x}_{p2}+1}\end{aligned} \tag{5}$$

$$\begin{aligned}\overline{\theta}_{g2} = \frac{\theta_{g2}k_2\lambda_2^{n_2-1}}{A_{L2}} = \frac{-2(\bar{x}_{p2}+1)[\bar{x}_{p2}+1)]}{\bar{x}_{p2}+1}\left[\frac{\bar{x}_{p2}^2}{(n_2+1)(n_2+2)} + \frac{\bar{x}_{p2}}{(n_2+1)} + \frac{1}{2}\right]\bar{x}_{p2}^{n_2} \\ + \frac{4\bar{x}_{p2}^2 + 4(n_2+3)\bar{x}_{p2} + 2(n_2+2)(n_2+3)}{(n_2+1)(n_2+2)(n_2+3)}\bar{x}_{p2}^{n_2+1}\end{aligned} \tag{6}$$

And $\lambda_2 = (k_2/4E_PI_P)^{0.25}$, the reciprocal of characteristic length; I_p = moment of inertia of an equivalent solid pile; and $\bar{x}_{p2} = \lambda_2 x_{p2}$, normalised slip depth.

Deep Sliding

Opposite to the normal sliding, the condition of $L_1 > 1.2L_{c1}+x_{p1}$ warrants a deep (soil carrying piles) sliding mode to occur (see Fig. 1e). Eq. (2) may be used by neglecting rigid movement (i.e. $(L_1-x_s)\theta_o \approx 0$) and loading eccentricity ($e_{o2} \approx 0$). The mode is characterised by $H_1(x_{p1}) = |-H_2(x_{p2})|$ and $w_s = w_{g1}(x_{p1}) + w_{g2}(x_{p2})$, which may be resolved to gain the slip depth x_{p1} and x_{p2} (thus H_2, w_{gi}, and θ_{gi}) for the w_s, thus the pile response. This mode will be discussed elsewhere, owing to limited space.

E-E AND P-EP SOLUTIONS

Elastic (Sliding layer) - Elastic (Stable layer) (E-E) Solution

In the context of the load transfer model, the deflection w_{Bi} at depth z_i of an infinitely long pile in i^{th} layer with a constant k_i (see Fig. 1e) (Guo 2006) is given by:

$$w_{Bi}(z_i) = e^{-\alpha_i z_i}(C_{5i}\cos\beta_i z_i + C_{6i}\sin\beta_i z_i) \tag{7}$$

where

$$\alpha_i = \sqrt{\lambda_i^2 + N_{pi}/(4E_pI_p)} \quad \beta_i = \sqrt{\lambda_i^2 - N_{pi}/(4E_pI_p)} \tag{8}$$

Four conditions at the point O (see Table 2) are noted as

$$\theta_{g1}+\theta_o = -\theta_{g2},\ M_{o1} = M_{o2},\ H_1 = H, \text{ and } -H_2 = H \tag{9}$$

where the dragging effect is captured by the M_{oi}. The four equations were expanded and resolved (see Appendix I), which provide the four constants C_{51}, C_{52}, C_{61} and C_{62}.

$$C_{5i} = (-1)^i \frac{H}{4}\frac{2\alpha_i\alpha_j + 2\alpha_i^2 - \lambda_i^2 + \lambda_j^2}{\lambda_i^2(\alpha_i\lambda_j^2 + \alpha_j\lambda_i^2)E_pI_p} + \frac{\theta_o}{2}\frac{(2\alpha_i^2 - \lambda_i^2)\lambda_j^2}{\lambda_i^2(\alpha_i\lambda_j^2 + \alpha_j\lambda_i^2)} \tag{10}$$

$$C_{6i} = (-1)^i \frac{H}{4} \frac{\alpha_i(2\alpha_i^2 - 3\lambda_i^2 + \lambda_j^2) + 2\alpha_j(\alpha_i^2 - \lambda_i^2)}{\beta_i\lambda_i^2(\alpha_i\lambda_j^2 + \alpha_j\lambda_i^2)E_pI_p} + \frac{\theta_o}{2} \frac{(2\alpha_i^2 - 3\lambda_i^2)\alpha_i\lambda_j^2}{\beta_i\lambda_i^2(\alpha_i\lambda_j^2 + \alpha_j\lambda_i^2)} \quad (11)$$

where $i = 1, j = 2$ or $i = 2, j = 1$, respectively. Eq. (7) indicates the profiles of shear force $Q_{Bi}(z_i)$, bending moment $M_{Bi}(z_i)$, and slope $\theta_{Bi}(z_i)$ in either layer resemble those for active piles (e.g. Guo 2006). This solution accounts for the coupled effect (with $N_{pi} \neq 0$) among different soil layers, and is referred to as E-E(Coupled) solution. Otherwise, taking $N_{pi} = 0$ (thus $\lambda_i = \alpha_i = \beta_I$ from Eq. (8)), the solution reduces to the (uncoupled) E-E solution (Cai and Ugai 2003) (see Appendix I). Unfortunately, the input values of H_2 and θ_o for the E-E solutions are not known for a given soil movement w_s.

Plastic (Sliding layer) - Elastic-plastic (Stable layer) (P-EP) Solution

A plastic interaction with subsoil is normally expected in passive piles. In particular, concerning the normal sliding mode, and the p_{u1} profile for sliding layer, the plastic (P) solution (e.g. Eq. (3)) for the sliding layer is resolved together with an EP solution for the stable layer, using the interface conditions of Eq. (9). This is referred to as P-EP solution. The sliding resistance is given by Eq. (3), and the bending moment M_{o1} at the sliding level is obtained as

$$M_{o1} = 0.5A_{L1}[(x_s - 2L_1)x_s\xi + (L_1 - x_s)^2] \quad (12)$$

In the resistance zone ($x = 0 \sim x_s$), the shear force Q and bending moment M at depth x (measured from ground level) are given by

$$Q_{A1}(x) = \xi A_{L1}x \qquad M_{A1}(x) = 0.5\xi A_{L1}x^2 \quad (13a,b)$$

In the thrust zone ($x = x_s \sim L_1$), they are given by

$$Q_{A1}(x) = H_1 + A_{L1}(L_1 - x) \quad (14a)$$

$$M_{A1}(x) = -\frac{A_{L1}}{2}x^2 + (H_1 + A_{L1}L_1)x - \frac{(H_1 + A_{L1}L_1)^2}{2(1+\xi)A_{L1}} \quad (14b)$$

It should be stressed that Eq. (13) satisfies the conditions of zero bending moment and shear force at ground level. With Eq. (3), the M_{o1} from Eq. (12) is recast into

$$M_{o1} = \frac{H_1^2}{2A_{L1}}[1 - \frac{\xi}{1+\xi}(1 + \frac{A_{L1}L_1}{H_1})^2] \tag{15}$$

The moment M_{o1} is converted to H_2e_{o2} (see Fig. 1c) with due account of the moment caused by the distributed p_{u2} over the 'dragging' zone from depth L_1-e_{o2} to L_1 (Matlock et al. 1980; Guo 2009). The e_{o2} may be bracketed by Eq. (16) for a linear p_{u2} over the zone, and by Eq. (17) for a uniform p_{u2}:

$$e_{o2} = \sqrt[3]{\frac{3M_{o1}}{A_{L2}} + \sqrt{\left(\frac{-3M_{o1}}{A_{L2}}\right)^2 + \left(\frac{-2H_1}{A_{L2}}\right)^3}} + \sqrt[3]{\frac{3M_{o1}}{A_{L2}} - \sqrt{\left(\frac{-3M_{o1}}{A_{L2}}\right)^2 + \left(\frac{-2H_1}{A_{L2}}\right)^3}} \tag{16}$$

$$e_{o2} = [H_1 - \sqrt{H_1^2 - 2A_{L2}M_{o1}}]/A_{L2} \tag{17}$$

Unsure about the p_{u2} profile over the zone, the values of e_{o2} are estimated using Eq. (16) and (17) for each case study. They, however, offer only slightly different, but often negligible steps in the moment profile at the depth of L_1-e_{o2}. Thereby, the response profiles will be provided later only for those obtained using Eq. (16) (linear p_{u2}). The maximum bending moment in sliding layer is given by

$$M_{\max 1} = \frac{\xi(H_1 + A_{L1}L_1)^2}{2(1+\xi)^2 A_{L1}} \tag{18}$$

Dragging does not occur, so long as $M_{o1} = 0$ or $\xi = \xi_{min}$, as deduced from Eq. (15).

$$\xi_{\min} = 1/[(1 + \frac{A_{L1}L_1}{H_1})^2 - 1] \tag{19}$$

On the other hand, the M_{max2} from stable layer may move to sliding level and become the dragging moment M_{o1} of Eq. (15). Accordingly, the ξ attains a maximum value of ξ_{max}

(see later Case V). A complicated equation for ξ_{max} can be derived, but it is unnecessary, as it is more convenient to use

$$\xi_{\max} = 1/\xi_{\min} \tag{20}$$

Generally speaking, it follows $\xi = \xi_{min}$ for flexible piles, $\xi = \xi_{max}$ for rigid piles, and $\xi_{min} \le \xi \le \xi_{max}$ for upper rigid (in sliding layer) and lower (in stable layer) flexible piles.

The thrust H_2 is correlated to stable layer properties by the normalised $\overline{H}_2$

$$\overline{H}_2 = \frac{H_2 \lambda_2^{n_2+1}}{A_{L2}} = \frac{0.5\bar{x}_{p2}^{n_2}[(n_2+1)(n_2+2)+2\bar{x}_{p2}(2+n_2+\bar{x}_{p2})]}{(\bar{x}_{p2}+1)(n_2+1)(n_2+2)} \tag{21}$$

The prediction using P-EP solution is conducted via seven steps: (i) The parameters A_{Li}, L_1, k_2, and λ_2 are obtained along with $n_1 = 0$, and $n_2 = 1.0$; (ii) the ξ is stipulated as 0~0.8 for flexible piles or 3-6 for rigid piles as shown later; (iii) Let H_1 from Eq. (4) be equal to H_2 from Eq. (21) to gain a normalised slip depth $\bar{x}_{p2}$ for each soil movement w_s; (iv) The $\bar{x}_{p2}$ in turn permits the H_2, w_{g2}, and θ_{g2} to be calculated using Eqs. (21), (5) and (6) respectively for a given set of A_{Li} and n_i; (v) The values of M_{o1}, e_{o2}, ξ_{min}, and ξ_{max} are calculated using Eq. (15), Eq. (16), Eq. (19), and Eq. (20), respectively; (vi) The distribution profiles of the displacement, rotation, moment, and shear force in stable layer are obtained using Eqs. (13)-(14) and the EP solutions provided in Appendix I. (vii) Check whether the obtained moment profile is smooth over the dragging zone, if not, a new value of ξ may be assumed ($\xi_{min} \le \xi \le \xi_{max}$) and steps (iii)-(vii) are repeated. This process can be readily done using Mathcad^{TM} program. Note (1) using the EP solutions, the depth x_2 should be replaced with $x_2 - L_1 + e_{o2}$ (sliding layer), as the depth x_i is measured from the depth L_1 (see Fig. 1); and (2) the rigid rotation angle θ_o ($=-\theta_{g2}$) and the loading zone L_1-x_s ($= (w_s - w_{g2})/|\theta_{g2}|$) are readily obtained.

The solution is underpinned by a uniform soil movement profile (Fig. 1d), but it can be modified to accommodate other profiles through new geometric relationships rather than Eq. (4). The solution neglects the coupling impact, and the sliding friction (Guo 2006).

The main conditions and features of the P-EP solution are summarised in Table 2. The solution captures the impact of dragging using the eccentricity e_{o2}, and the parameter ξ. Conversely, matching measured profiles of bending moment, shear force and pile deflection (for a particular w_s) values of A_{Li} (or H_2), θ_o (or θ_{g2}), and ξ may be deduced, along with e_{o2} gained from measured M_{o1} and H_1 at sliding level using Eq. (16). Any differences from the E-E prediction allow the effect of plasticity (ξ and x_{p2}) and dragging (e_{o2}) to be identified as well. The proposed P-EP solution is elaborated via a design example.

In summary, the E-E(coupled), and P-EP solutions are developed using the compatible conditions of Eq. (9), and $L_2 > L_{c2}+x_{p2}$ (see Table 2). The solutions were all entered into a program called GASMove operating in the mathematical software Mathcad^{TM}. The GASMove was used to gain numeric values presented subsequently.

Design Charts

Slope stabilising piles predominately work in the normal sliding mode, which may be simply modelled by using the P-EP solution with $n_1 = 0$, $n_2 = 1.0$, $e_{oi} = 0$, and $\xi = 0$ (for non-dragging case). Given a relative layer stiffness $(A_{L2}/A_{L1})/\lambda_2^{n2}$, for each normalised soil movement $\overline{w}_s$ ($=w_s k_2 \lambda_2^{n_2} / A_{L2}$), Eq. (4) was used to obtain the displacement ratio w_s/w_{g2}, the normalised load $\overline{H}_2$, moment $\overline{M}_{max\,2}$ ($=M_{max\,2}\lambda_2^{n_2+2}/A_{L2}$) and slope $\overline{\theta}_{g2}$. Repeating the

calculation for a series of $\overline{w}_s$ allows the nonlinear response to be obtained for each of the six layer stiffnesses of 1, 2, 4, 6, 8, or 10. The results gained are plotted in

- Fig. 2 in form of the normalised load ($\overline{H}_2$) versus displacement ($\overline{w}_{g2}$) curves, which are independent of the layer stiffness;
- Fig. 3a, b, c, d, and e, showing the curves of $\overline{w}_s \sim w_s/w_{g2}$, $\overline{H}_2 \sim w_s/w_{g2}$, $-\overline{\theta}_{g2} \sim w_s/w_{g2}$, $\overline{M}_{max\,2} \sim w_s/w_{g2}$, and the evolution of the normalised slip depth $\bar{x}_{p2}$, respectively, and
- Fig. 4 regarding the impact of $n_2 = 0.7 \sim 1.7$ ($n_1 = 0$) on the normalised response.

These figures may be employed to calculate the pile response for a known w_s, although the w_{g2} and H_2 at sliding level may be overestimated without the dragging impact ($e_{o2} = 0$, on safe side). The use of $n_1 = 0$ has limited impact on the overall prediction (see Fig. 3f), but it allows the shape of measured moment profiles to be well modelled.

Nonhomogeneous p_{u2} (Current) or k (Numerical) Based Solutions

The current solutions are underpinned by a non-homogenous p_{u2} and a uniform k_2, while existing numerical solutions are generally based on a non-homogenous k_2, and a uniform p_{u2} (Poulos 1995; Chow 1996). The two types of solutions are compared next in light of a normal sliding Case I (Esu and D'Elia 1974).

A reinforced concrete pile was installed in a sliding clay slope, which has an outside diameter d of 0.79 m, a length L of 30 m, and a bending stiffness E_pI_p of 360 MNm^2. The 'ultimate' shear forces, bending moments, and deflections were measured along the pile (Esu and D'Elia 1974), which are plotted in Fig. 5. Chen and Poulos (1997) conducted a simplified boundary element analysis (BEA) on the pile using $E_{si} = 0.533x$ (MPa, x measured from ground level, and $n_2 = 1.0$), $s_{ui} = 40$ kPa, $p_{u1} = 3ds_{u1}$, $p_{u2} = 8ds_{u2}$,

and w_s = 110 mm uniform to the sliding depth of 7.5 m. The predicted bending moments, deflections and shear forces are plotted in Fig. 5 along with the measured data.

The GASMove predictions were made by taking A_{L1} = 94.8 kN/m (= 3*40*0.79 kPa, N_{g1} = 3.0), A_{L2} = 52 kPa (N_{g2} = 1.3), ξ = 0.5, n_1 = 0, n_2 = 1.0, k_1 = 2.5MPa and k_2 = 7MPa. The low p_{u2} (compared to p_{u1}) resembles that for embankment piles (Stewart et al. 1994), as is seen again later in Cases VII and VIII. The k_i was deduced from $G_{si} = 54.8 s_{ui}$ and k_i/G_{si} = 3.65, with the latter being obtained using k_{1i} = 1.5 (Table 1, for e_{oi}/d = 2~3), γ_i = 0.164, and E_p/G_{si} = 8,589. The critical length L_{ci} is estimated as 8.1 m (higher than 7.7 m obtained using k_i/G_{si} = 3, see Table 3). The P-EP and E-E solutions were obtained, and are plotted in Fig. 5. They agree well with the measured data and the BEA. In particular, with $L_1 < L_{c1}$, the pile deflection is equal to the sum of the deflection w_{g2} and the rigid rotation $\theta_o(L_1-x)$.

Guo (2003), in light of the P-EP solution, predicted the profiles for the stable layer using each of the three pairs of parameters A_{L2} and n_2 provided in Fig. 6 (with a uniform subgrade modulus k_2, and ignoring any resistance above the depth x_s). The results are compatible with the BEA, and with the measured deflection, rotation and bending moment, respectively. The shear force profile is well replicated using n_2 = 1.0, with which the BEA solutions were obtained, and resulted in the lowest thrust instead (otherwise, e.g. H_2 = 458.6 at n_2 = 0.5). A typical calculation is elaborated next.

A Design Example using P-EP solution

The Case I pile response is predicted using the design charts for ξ = 0. With E_pI_p = 360 MNm^2, k_i = 8MPa and w_s =110 mm, it follows λ_i = 0.273 [= $(8/4*360)^{0.25}$], $(A_{L2}/A_{L1})*\lambda_2^{(n1-n2)}$ = 2.01, and $\overline{w}_s$ = 4.62 (= 0.11*8,000*0.273/52).

The layer stiffness and $\overline{w}_s$ correspond to w_s/w_{g2} = 1.836 (see Fig. 3a), which in turn gives $\overline{H}_2$ = 0.49 (Fig. 3b), $\overline{\theta}_{g2}$ = -2.136 (Fig. 3c), and $\overline{M}_{\max 2}$ = 0.32 (Fig. 3d). Consequently, the w_s =110 mm induces H = 342 kN, w_{g2} = 59.9 mm, M_{max2} = 816.8 kNm, and θ_{g2} = -0.0139, which are ~15% larger than 316.15 kN, 52.1 mm, 739.0 kNm and θ_{g2} = -0.012, obtained using ξ = 0.5 and GASMove, and on the safe side. This example also indicates that the accuracy of ξ generally is not critical, as is noted later for all other cases.

With θ_o = 0.012, θ_{g2} = 0.012, and H_1 = 316.15 kN, A_{L1} = 94.8 kPa (thrust), and ξ = 0.5 (resistance), the response profiles are obtained using the P-EP solution provided in Appendix I. The depth x_s is obtained as 2.78 m using Eq. (3), and the M_{o1} and the e_{o2} as 253.07 kNm and 0.93 m using Eq. (15), and Eq. (16), respectively. The bending moment and shear force profiles in sliding layer are obtained using Eqs. (13) and (14). The pile movement is taken as $w_{g2}+\theta_{g2}(L_1-x)$, which is identical to the GASMove prediction (see Fig. 5(b)). With n_2 = 1, and A_{L2} = 52 kPa, the slip x_{p2} was estimated as 2.96 m using Eq. (21), which gives $F(2,0)=F(1,0)=0$, $w''_{p2}=1.976\times10^{-3}$, $w'''_{p2}=2.443\times10^{-4}$ and

$$w_{B2}(z_2) = e^{-\lambda_2 z_2}(0.01926\cos\lambda_2 z_2 - 0.01325\sin\lambda_2 z_2) \tag{22}$$

$$-M_{B2}(z_2) = E_p I_p e^{-\lambda_2 z_2}[1.976\times10^{-3}\cos\lambda_2 z_2 + 2.871\times10^{-3}\sin\lambda_2 z_2] \tag{23}$$

$$-M_{A2}(x_2) = [-\frac{x_2^{\,n_2+2}}{(n_2+2)(n_2+1)}A_{L2} + H_2 x_2] + M_{o2} \tag{24}$$

These equations offer (1) $w_{B2}(0)= w_{g2}$ = 52.1 mm at z_2 = 0 of the stable layer; and (2) M_{max2} = -739.04 kNm that occurred at 3.631 m (= x_{p2} of 2.963 + z_{max2} of 0.669). The bending moment profile obtained is subsequently shifted upwards by replacing x_2 with $x_2-L_1+e_{o2}$ (stable layer, $z_2 = x_2-x_{p2}$), so is the shear force profile. This results in smooth bending moment and shear force profiles (across the sliding interface).

The calculation should be repeated for other values of w_s to gain H, w_{g2}, M_{max} and θ_{g2}, which allow nonlinear curves of H~w_s, H~w_{g2}, H~M_{max} and H~θ_{g2} to be gained for the pile in a manner adopted for lateral piles (Guo 2006)

CASE STUDY

The current E-E and P-EP solutions were employed to study seven instrumented piles termed as Cases II-VIII. The pile and soil properties are summarised in Table 3, including the outside diameter d, wall thickness t, Young's modulus E_p, thicknesses of sliding layer L_1/stable layer L_2, and SPT blow counts N_i and/or undrained shear strength $s_{ui,}$ etc. The profiles of bending moment and deflection were reported for all cases, but those of the shear force are available only for Cases I, VI and VII. They are plotted in Figs. 7-11. The critical pile lengths L_{c1}/L_{c2} were calculated using a k_i of $3G_{si}$. The angle θ_o, and the thrust H were deduced using the E-E solution and the measured response. They are tabulated in Table 3 as well. As for the P-EP solution, the input parameters A_{Li}, k_i, w_s, and ξ along with n_1=0, and n_2= 1 are given in Table 4, so are the calculated values of e_{o2}, x_s, x_{p2}, H_2, θ_o, $w_{g2,}$ λ_2, ξ_{min} and ξ_{max}. Each case is briefly described next.

Long, Short Piles, θ_o Negative and Plasticity (Cases II - VI)

Steel piles in Cases II-V all have d = 318.5 mm, t = 6.9 mm, E_P = 210 GPa, and k_i = 0.64N_i and respective measured H_2 and θ_o (Cai and Ugai 2003). They were predicted using the P-EP solution, with the k_i and an A_{Li} of (3.4~8.5)N_i kN/m (see Table 4). In Hataori landslide, two rows of the steel pipe piles (at a center-center spacing of 12.5d) were installed to 24 m (= L), to stabilise the active slide occurred at L_1 =11.2 m (Case II), and to 17 m (= L) at another location of the slide at L_1 = 8m (Case III). The predicted H_2 of 139.1 kN, and θ_o of 0.029 for a uniform w_s of 153 mm (see Fig. 7a and b, Case II) are

close to the measured 150 kN and 0.026, respectively; so are the predicted H_2 of 69.6 kN and θ_o of 0.0085 at w_s = 27 mm (see Fig. 7c and d, Case III) compared to the measured 70 kN and 0.004, respectively.

In the Kamimoku Landslide, the piles were configured to a column and a row spacing of 4 m and 2 m, respectively, and installed to 14 m deep to arrest the slide at L_1 = 6.5m (Case IV). The predicted H_2 of 123.3 kN at w_s = 150 mm (see Fig. 8a and b) agree with 139.1 kN noted in the similar Case II, but the H_2 was 'overestimated' as 300 kN using an 'abnormal' negative θ_o (Cai and Ugai 2003). Rotation is not included in the deflection profile (see Fig. 8b) for this deep sliding case.

In the Kamimoku Landslide, the piles were installed to a depth of 10 m, to arrest the sliding at L_1 = 4 m (Case V). The predicted H_2 of 253.7 kN and θ_o of 0.054 at w_s = 320 mm (see Fig. 8c and d) compare well with the measured 250 kN and 0.04 respectively, although the pile was short in both layers.

Reinforced piles (with d = 300 mm, t = 60 mm, and L =10 m) failed at L_1 = 7.3 m in the Katamachai Landslide (Case VI) with s_{u1} = 30 kPa, and N_2 (SPT) =16.7. Using k_1= $200s_{u1}$, k_2 = $0.6N_2$, N_{g1}= 2.2, and A_{L2} =$2.37N_2$ kN/m^2, the P-EP solution predicts H_2 = 59.1 kN and θ_o = 0.0234 at w_s = 135 mm (see Fig. 9), which are in close proximity to the measured 51 kN, and 0.025, respectively, in spite of underestimating the pile deflection.

Plastic Hinge (Case VII)

A reinforced concrete pile (d =1.2 m and L = 22 m) was bored into a slope with s_{ui} = 30 kPa (Carrubba et al. 1989). A slide occurred at L_1 = 9.5 m and with a 2 m transition layer (see Fig. 10a and c), and caused a plastic hinge in the pile at a depth of 12.5 m. The P-EP prediction was made using (Chen and Poulos 1997) (1) $k_i \approx$ 15 MPa (= $500s_{ui}$); (2)

E_pI_p = 2,035.8 MNm^2 (with E_p being taken as 20 GPa); (3) A_{L1} =198 kN/m (N_{g1}= 5.5), and A_{L2} = 79.6 kN/m^2 (N_{g2}= 2.65); and (4) A uniform w_s of 95 mm to a depth of 7.5 m. The pile observes normal sliding mode (see Table 4), and the P-EP prediction compares well with the measured response including the depth of the plastic hinge (at the M_{max}).

Piles -Retaining Wall –Excavation (Case VIII)

A model single pile located at 3 m behind a retaining wall was tested at 50g in centrifuge (Leung et al. 2000), to simulate a bored pile, 0.63 m in diameter, 12.5 m in length, and 220 MNm^2 in flexural stiffness E_pI_p. The sand has a unit weight of 15.78 kN/m^3; a relative density of 90%; an angle of internal friction of 43°; and an average E_s of 27 MPa (with Poisson's ratio ν_s = 0.4, E_s = 6x MPa) over a sliding depth of 4.5 m (at which sand moves significantly).

The P-EP predictions were made in light of (see Table 4) A_{L1} = 37.8 kN/m, A_{L2} = 18.9 kN/m^2, ξ = 0, L_1 = 4.5 m, and w_s = 4.5, 6.0 or 7.3 mm for the excavation depths of 2.5, 3.5 or 4.5 m, respectively. In particular, the input free-field w_s was gained using the measured w_s (14 mm at the surface and linearly reduced to zero at a depth of 7.5 m), as recorded at 3 m from the wall following the excavation to 4.5 m.

The predicted bending moment and deflection profiles agree with the measured ones for the three excavation depths (see Fig. 11). The slip depth x_{p2} was 1.8~2.23 m, which renders limited impact of the p_{ui} (compared to the modulus k_i) on the prediction. With $L_i < L_{ci}$ (= 23.1 m), the pile is rigid in either layer. The E-E solution is not applicable, and offers divergent predictions against the measured data.

Remarks on Case Study

Normalised bending moment $\overline{M}_{max2}$, sliding thrust $\overline{H}_2$, and rigid rotational angle $\overline{\theta}_2$ were calculated for each case using the values of M_{max2}, H_2, λ_2, k_2, n_2 in Table 4 and

θ_{g2} (not shown herein, but can be deduced from Table 3). The pairs of $\overline{M}_{\max 2}$ vs $\overline{H}_2$, and $\overline{M}_{\max 2}$ vs $\overline{\theta}_{g2}$ are plotted in Fig. 12a, and Fig. 12b, respectively, along with the P-EP predictions, which indicate a sufficient accuracy of the P-EP solution.

Tables 3 and 4 generally indicate slightly different values of θ_o between the E-E and P-EP solution for all piles in normal sliding mode, as is the case for the thrust *H*. The main features from this study on the instrumented piles (Cases I-VI) are as follows.

(1) Exhibiting deep sliding mode, the measured response of Case IV pile is well predicted using the E-E solution, and it is the only case with $M_{max1}>M_{max2}$.

(2) All piles but for Case IV worked in normal sliding mode.

- That the two piles rotated rigidly in sliding layer in Cases II and VI (see Tables 3 and 4) legitimizes the new critical length of $1.2L_{c1}+x_{p1}$.
- The P-EP solutions (n_2 = 1.0) generally well predict the moments and deflections (Figs. 7~11) by using $\theta_o = -\theta_{g2}$ (see Table 4), but for the deflection in Case VI, and $M_{max1}< M_{max2}$.
- The value of ξ varies as follows: (1) $\xi = \xi_{min}$ if $\xi_{max}- \xi_{min} > 20$ (flexible piles); (2) $\xi = \xi_{max}$ if $\xi_{max}- \xi_{min} < 7$ ('rigid' piles in both layer); and (3) $\xi = \xi_{min} \sim \xi_{max}$ if $7 \le \xi \le 20$.

It is deemed sufficiently accurate to determine A_{Li}, and k_i (or G_{si}) using the instructions for active piles to passive piles. The p_{ui} and k_i may differ from those adopted in other methods (Stewart et al. 1994; Chen et al. 2002; Cai and Ugai 2003), but the associated impact is limited, so long as the total resistance over the slip depths is of similar magnitude, as with laterally loaded piles.

CONCLUSIONS

New E-E and P-EP solutions are established for passive piles and presented in closed-form expressions. The P-EP solutions are complied into a program called GASMove and presented in non-dimensional charts. The solutions are used to study eight instrumented piles, which show the following:

(1) The proposed H and w_s relationship of Eq. (4) works well, although underpinned by a uniform soil movement profile. The obtained angle θ_o and shear force H are generally slightly different between the P-EP solution and the E-E solution, respectively.

(2) The P-EP solution well captures the pile response under normal sliding mode (with $L_1<L_{c1}$ and $L_2>L_{c2}$); and the E-E solution works well for 'deep sliding' mode, in light of input soil parameters G_{si} (for k_i), ξ, w_s, L_1, and A_{Li} (for p_{ui}). Similar predictions may be gained from different set of p_u and k profiles, as with laterally loaded piles.

(3) The solutions are readily evaluated using professional math programs (e.g. Mathcad^{TM}). The design charts allow nonlinear response to be hand-calculated.

Finally, to improve our understanding about passive piles, pile tests should provide both bending moment and shear force profiles for each magnitude of soil movement w_s.

REFERENCES

Byrne, P. M., D. L. Anderson and W. Janzen (1984). "Response of piles and casings to horizontal free-field soil displacements." Canadian Geotechnical Journal 21(1): 720-725.

Cai, F. and K. Ugai (2003). "Response of flexible piles under laterally linear movement of the sliding layer in landslides " Canadian Geotechnical Journal 40(1): 46-53.

Carrubba, P., M. Maugeri and E. Motta (1989). Esperienze in vera grandezza sul comportamento di pali per la stabilizzaaione di un pendio. Proceedings of XVII Convegno Nazionale di Geotechica, Assn. Geotec, Italiana.

Chen, C.-Y. and G. R. Martin (2002). "Soil-structure interaction for landslide stabilizing piles." Computers and Geotechnics 29(5): 363-386.

Chen, L. T. and H. G. Poulos (1997). "Piles subjected to lateral soil movements." Journal of Geotechnical and Geoenvironmental Engineering, American Society of Civil Engineers 123(9): 802-811.

Chen, L. T., H. G. Poulos, C. F. Leung, Y. K. Chow and R. F. Shen (2002). "Discussion of "Behavior of pile subject to excavation-induced soil movement."." Journal of Geotechnical and Geoenvironmental Engineering, American Society of Civil Engineers 128(3): 279-281.

Chmoulian, A. (2004). "Briefing: Analysis of piled stabilization of landslides." Proceedings of the Institution of Civil Engineers, Geotechnical Engineering 157(2): 55-56.

Chow, Y. K. (1996). "Analysis of piles used for slope stabilization." International Journal for Numerical and Analytical Methods in Geomechanics 20(9): 635-646.

Choy, C. K., J. R. Standing and R. J. Mair (2007). "Stability of a loaded pile adjacent to a slurry-supported trench." Geotechnique 57(10): 807-819.

De Beer, E. and R. Carpentier (1977). "Discussion on 'Methods to estimate lateral force acting on stabilising piles' By Ito, T., and Matsui, T. (1975)." Soil and Foundations 17(1): 68-82.

Esu, F. and B. D'Elia (1974). "Interazione terreno-struttura in un palo sollecitato dauna frana tipo colata." Rivista Italiana di Geotechica. 111(?): 27-38.

Frank, R. and P. Pouget (2008). "Experimental pile subjected to long duration thrusts owing to a moving slope." Geotechnique 58(8): 645-658.

Fukuoka, M. (1977). The effect of horizontal loads on piles due to landslides. Proceedings 9th International Conference on Soil Mechanics and Foundation Engineering, Speciality session 10, Tokyo.

Guo, W. D. (2003). A simplified approach for piles due to soil movement. Proceedings of 12th Panamerican conference on soil mechanics and geotechnical engineering, Cambridge, Massachusettes, USA, Verlag Gluckauf GMBH. Essen (Germany).

Guo, W. D. (2006). "On limiting force profile, slip depth and lateral pile response." Computers and Geotechnics 33(1): 47-67.

Guo, W. D. (2009). "Nonlinear behaviour of laterally loaded fixed-head piles and pile groups." International Journal for Numerical and Analytical Methods in Geomechanics 33(7): 879-914.

Guo, W. D. (2010). Predicting non-linear response of laterally loaded pile groups via simple solutions. Advances in Analysis, Modeling, & Design, Proceedings of the GeoFlorida 2010 Conference, GSP 199, Florida, ASCE.

Guo, W. D. and E. H. Ghee (2004). Model test on single piles in sand due to soil movement. Proceedings 18th Australian Conference on the Mechanics of Structures and Materials, Perth, Australia, Balkema, Netherlands.

Guo, W. D. and F. H. Lee (2001). "Load transfer approach for laterally loaded piles." International Journal for Numerical and Analytical Methods in Geomechanics 25(11): 1101-1129.

Guo, W. D. and H. Y. Qin (2010). "Thrust and bending moment of rigid piles subjected to moving soil." Can. Geotech. J. 47(2): 180-196.

Henke, S. (2009). "Influence of pile installation on adjacent structures " International Journal for Numerical and Analytical Methods in Geomechanics 34(11): 1191-1210.

Ito, T. and T. Matsui (1975). "Methods to estimate lateral force acting on stabilising piles." Soils and Foundations 15(4): 43-59.

Leung, C. F., Y. K. Chow and R. F. Shen (2000). "Behaviour of pile subject to excavation-induced soil movement." Journal of Geotechnical and Geoenvironmental Engineering, American Society of Civil Engineers 126(11): 947-954.

Matlock, H. (1970). Correlations for design of laterally loaded piles in soft clay. Proceedings 2nd Annunal Offshore Technology Conference, OTC1204, Dallas, Texas.

Matlock, H., B. Wayne, A. E. Kelly and D. Board (1980). Field tests of the lateral load behaviour of pile groups in soft clay. Paper No. OTC. 3871, Proceedings of 12th annual offshore technology conference, Houston, Texas.

Mostafa, Y. E. and M. H. E. Naggar (2006). "Effect of seabed instability on fixed offshore platforms." Soil Dynamics and Earthquake Engineering 26(?): 1127-1142.

Murff, J. D. and J. M. Hamilton (1993). "P-Ultimate for undrained analysis of laterally loaded piles." Journal of Geotechnical Engineering, American Society of Civil Engineers 119(1): 91-107.

Potts, D. M. (2003). "Numerical analysis: a virtual dream or practical reality?" Geotechnique 53(6): 535-573.

Poulos, H. G. (1995). "Design of reinforcing piles to increase slope stability." Canadian Geotechnical Journal 32(5): 808-818.

Randolph, M. F. and G. T. Houlsby (1984). "The limiting pressure on a circular pile loaded laterally in cohesive soil." Geotechnique 34(4): 613-623.

Smethurst, J. A. and W. Powrie (2007). "Monitoring and analysis of the bending behaviour of discrete piles used to stabilise a railway embankment." Geotechnique 57(8): 663-677.

Springman, S. M. (1989). Lateral loading on piles due to simulated embankment contstruction, University of Cambridge. Ph. D Thesis.

Stewart, D. P., R. J. Jewell and M. F. Randolph (1994). "Design of piled bridge abutments on soft clay for loading from lateral soil movements." Geotechnique 44(2): 277-296.

Viggiani, C. (1981). Ultimate lateral load on piles used to stabilise landslide. Proceedings 10th International Conference on Soil Mechanics and Foundation Engineering, Stockholm, Sweden.

Yang, Z. and B. Jeremic (2002). "Numerical analysis of pile behaviour under lateral load in layered elastic-plastic soils." Int. J. Numer. and Anal. Meth. in Geomech. 26(14): 1385-1406.

NOMENCLATURE

A_{Li} = coefficient for the LFP for the ith layer [FL^{-1-ni}];

d = outside diameter of a cylinder pile [L];

e_{oi} = distance from point O to incorporate dragging effect [L];

E_p = Young's modulus of an equivalent solid cylinder pile [FL^{-2}];

E_{si} = Young's modulus of soil [FL^{-2}];

G_{si}, G_{si}^* = shear modulus of the soil [FL^{-2}], and $G_{si}^* = (1+3\nu_{si}/4)G_{si}$, respectively;

H_2 = lateral load applied at a distance of 'e_{o2}' above point O, and $H_1 = -H_2$ [L];

i = subscript 1, and 2 denoting the upper sliding and lower stable layer, respectively;

I_p = moment of inertia of an equivalent solid cylinder pile [L^4];

k_i = modulus of subgrade reaction [FL^{-2}];

k_{1i}, k_{ri} = parameters for estimating the load transfer factor, γ_i of flexible and rigid piles, respectively.

K_{pi} = $\tan^2(45^o + \phi_{si}'/2)$, the coefficient of passive earth pressure;

$K_{ji}(\gamma)$ = modified Bessel function of second kind of j^{-th} order (j= 0, 1) for i^{-th} layer;

L, L_i = embedded pile length [L], and the thickness in the ith layer;

L_{ci} = critical embedded pile length in ith layer, beyond which the pile is classified as infinitely long [L];

LFP = net limiting force profile [FL^{-1}];

$M_{Ai}(x_i)$, $M_{Bi}(z_i)$ = moment induced in a pile element at a depth of 'x_i' in plastic zone [FL], and a depth of 'z_i' in elastic zone, respectively [FL];

M_{maxi} = maximum bending moment within a pile in ith layer [FL];

M_{oi} = $H_i e_{oi}$, bending moment about point O [FL];

n_i = power for the LFP;

N_i = blow count of the SPT;

N_{gi} = gradient correlated soil undrained strength with the limiting pile-soil pressure;

N_{pi} = fictitious tension for a strectched membrane used to tie together the springs around the pile shaft;

$Q_{Ai}(x_i)$, $Q_{Bi}(z_i)$ = shear force induced in a pile element at a depth of 'x_i' in plastic zone, and a depth of 'z_i' in elastic zone, respectively [F];

p_i, p_{ui} = force per unit length on pile shaft and limiting p_i [FL^{-1}];

s_{ui} = undrained shear strength of the i^{th} layer soil [FL^{-2}];

t = wall thickness of a pipe pile [L];

x = depth measured from ground level [L];

x_i = depth measured from point O on the sliding interface [L];

x_{maxi} = depth of maximum bending moment measured from point O in plastic zone [L];

x_{pi} = slip thickness from the elastic - plastic boundary to point O [L];

x_s = thickness of the zone, in which pile deflection exceeds soil movement [L];

w_i = lateral deflection of either w_{Ai} or w_{Bi} [L];

w_{Ai}, w_{Bi}= lateral deflection in the upper plastic and lower elastic zone, respectively [L];

w_{Bi}^{IV}, $w_{Bi}^{'''}$, $w_{Bi}^{''}$, $w_{Bi}^{'}$ = fourth, third, second and first derivatives, respectively of deflection w with respect to the depth x [L];

w_{gi} = lateral pile deflection at point O [L];

w_s = lateral (uniform) soil movement [L];

z_{max2} = depth of M_{max2} measured from the slip depth, x_{p2} [L];

z_i = x_i-x_{pi}, depth measured from the slip depth, x_{pi} [L];

α_i, β_i = the reciprocals of modified characteristic lengths [L];

γ_i = load transfer factor;

γ'_{si} = effective density of the overburden soil [FL^{-3}];

λ_i = the reciprocal of characteristic length [L^{-1}];

ν_{si} = Poisson's ratio of soil;

ξ = a factor used to capture the combined impact of pile-head constraints and soil resistance, etc on magnitude of resistance in resistance zone;

ξ_{max}, ξ_{min} = the maximum and minimum values of the factor ξ;

ϕ_{si}' = effective frictional angle of soil;

$\theta_{Ai}(x_i)$, $\theta_{Bi}(z_i)$ = rotational angle of a pile element at a depth of 'x_i' in plastic zone, and a depth of 'z_i' in elastic zone, respectively

θ_{gi} = rotational angle of a pile at point O;

θ_o = differential angle of the pile between upper and lower layer at point O;

Figure Captions

Fig.1. An equivalent load model for a passive pile: (a) The problem, (b) The imaginary pile, (c) Equivalent load H_2 and eccentricity e_{o2}; (d) Normal sliding, and (e) Deep sliding

Fig.2. Response of piles in normal sliding mode

Fig.3. Normalised ile response in stable layer owing to soil movement w_s ($n_2 = 1$, $n_1 = 0$, $e_{o2} = 0$, $\xi = 0$): (a) Soil movement, (b) Load, (c) Slope, (d) Maximum moment, (e) Slip depth, and (f) Schematic stress distributions

Fig. 4. Effect of soil profile ($n_2 = 0.7$~1.7, $n_1 = 0$, $e_{o2} = 0$, $\xi = 0$) on normalized pile response in stable layer: (a) Soil movement, (b) Load, (c) Slope, and (d) Maximum moment

Fig.5. Predicted (using $\theta_o = -\theta_{g2}$) vs. measured (Esu and D'Elia 1974) responses (Case I): (a) bending moment, (b) pile deflection, and (c) shear force

Fig. 6. Effect of n_2 and A_{L2} (n_2/A_{L2} = 0./120; = 0.5/51.0, and 1.0/ 25.0; A_{L2} in kPa) on the predicted pile response (Case I) in stable layer: (a) pile deflection, (b) shear force, (c) pile rotation, and (d) bending moment

Fig. 7. Predicted versus measured pile responses: (a) moment and (b) deflection for Case II, (c) moment and (d) deflection for Case III

Fig. 8. Predicted versus measured pile responses: (a) moment and (b) deflection for Case IV, (c) moment and (d) deflection for Case V

Fig. 9. Predicted (using $\theta_o = -\theta_{g2}$) vs. measured responses (Case VI): (a_1) bending moment, (b_1) deflection and (c_1) shear force at $w_s = 7.2$ mm; (a_2), (b_2) and (c_2) for $w_s = 24$ mm; and (a_3), (b_3) and (c_3) for $w_s = 135$ mm

Fig. 10. Predicted (using $\theta_o = -\theta_{g2}$) versus measured (Carrubba et al. 1989) pile responses (Case VII): (a) bending moment, (b) pile deflection, and (c) shear force

Fig. 11 Predicted versus measured pile response during excavation (Leung et al. 2000) (Case VIII): (a_1) deflection and (b_1) bending moment at 2.5 m; (a_2) deflection and (b_2) bending moment at 3.5 m; and (a_3) deflection and (b_3) bending moment at 4.5 m

Fig. 12. Predicted versus measured pile responses for all cases: (a) Normalized load versus moment, and (b) Normalized rotation angle versus moment

Table 1 Load transfer model for free-head single piles (Guo 2006)

Parameters N_{gi}, and n_i for the p_{ui}	G_{si}, L_{ci}, k_i, and N_{pi}
(1) Maximum x_{pi} = 8d (in-situ) and 20d (model piles), respectively. (2) Cohesive soil: N_{gi} = 0.6-6 (normal sliding), or 9-11.9 (deep sliding), $A_{Li} = N_{gi} s_{ui} d^{1-n_i}$. n_i = 0.7, and 1.7 for a uniform and a sharp increasing s_{ui} profile, respectively. $p_{ui} \le 11.9 s_{u\max i} d$. Given n_i = 0, it follows $p_{ui} = s_{ui} N_{gi} d$. (3) Cohesionless soil: $N_{gi} = s_{gi} K_{pi}^2$, n_i =1.7, $A_{Li} = N_{gi} \gamma_{si}' d^{2-n_i}$, where $K_{pi} = \tan^2(45^o + 0.5\phi_{si}')$, ϕ_{si}' = average effective frictional angle of soil, s_{gi} = 0.3-2.0 (an average of 1.12), γ_{si}' = effective unit weight of soil. (4) Layered soil: As a weak layer is adjacent to a stiff one, the p_u for the weak one increases by 40%, and for the stiff one reduces by 30%. n_i is 0.7-1.7. (5) The p_{ui} may be directly deduced from p_i-y_i curves. The N_{g2}, and n_2 may be deduced by matching closed-form solutions with 3 measured responses of *displacement, rotation and* moment profiles etc. for a passive pile. The p_{ui} should be reduced for excavation related piles.	(a) G_{si}= (25-340)s_{ui} with an average G_{si} of 92.3s_{ui}. G_{si}= (0.25-0.62)N_i(MPa) an average of 0.5N_i (MPa). (b) $L_{ci}/d = 1.05[\frac{E_p}{G_{si}}]^{0.25}$ (c) k_i = (2.4-3.9)G_{si} with an average of 3G_{si} (clay) and 3.2G_{si} (sand). Or k_i = (0.6-2.4)N_i k_i/G_{si} and $4N_{pi}/(\pi d^2 G_{si})$ are estimated using the expressions in the 'Note'

Note: In gaining p_{ui}, undrained shear strength s_{ui}, blow count of SPT, N_i, and effective angle of friction of soil ϕ_{si}' are averaged over the maximum slip depth x_{pi}. The G_{si} is an average value over the critical pile length L_{ci} .

$$\frac{k_i}{G_{si}} = \frac{3\pi}{2}\left\{2\gamma_i \frac{K_{1i}(\gamma_i)}{K_{0i}(\gamma_i)} - \gamma_i^2\left[\left(\frac{K_{1i}(\gamma_i)}{K_{0i}(\gamma_i)}\right)^2 - 1\right]\right\} \text{ and } \frac{4N_{pi}}{\pi d^2 G_{si}} = [K_{1i}(\gamma_i)/K_{0i}(\gamma_i)]^2 - 1$$

where $K_{ji}(\gamma_i)$ is modified Bessel function of second kind of j^{th} order (j = 0, 1) (Guo and Lee 2001) . The factor γ_i is given by $\gamma_i = k_{1i}(E_p/G_{si}^*)^{-0.25}$ for $L_1 > 1.2L_{c1}+x_{p1}$ or $L_2 > L_{c2}+x_{p2}$, otherwise $\gamma_i = 0.5k_{ri}d/L$, for rigid piles, where k_{1i} = 1.0 for a lateral load (e_{oi} = 0) applied at point O (sliding level), and k_{1i} = 2.0 for a pure moment; with k_{ri} = 2.14 (e_{oi}=∞) and 3.8 (e_{oi}= 0), respectively. G_{si}^*= (1+3ν_{si}/4)G_{si}, ν_{si} = soil Poisson's ratio.

Table 2 Conditions and salient features for various solutions

Solutions	Input parameters	w_s profile	Common conditions	Moment M_{oi}	Comments
E-E (Fukuoka (Fukuoka 1977), Cai & Ugai (Cai and Ugai 2003))	G_{s1}, G_{s2}, H_i, and θ_o. H_i & θ_o *assumed or measured*	Uniform w_s (θ_o= 0) Linear w_s, and the gradient of soil movement inclination θ_o ($\neq 0$)	Slope θ_{g1}, θ_{g2} satisfying $\theta_{g1}+\theta_o=-\theta_{g2}$ $H_1=H$ $H_1=\lvert -H_2\rvert$ and $L_2>L_{c2}+x_{p2}$	$M_{o1}=M_{o2}$	• $L_1>1.2L_{c1}+x_{p1}$; • Independent of w_s; • A given sliding depth e.g. Cases II and III
E-E (coupled)	G_{si}, ξ, w_s, L_1, and A_{Li} (n_1 = 0, and n_2 = 1.0 for P-EP; ξ = 0 for E-E)	$w_s=(L_1-x_s)\theta_o+w_{g1}+w_{g2}$ Deep sliding: $\theta_o\approx 0$ Normal sliding: $\theta_o\approx-\theta_{g2}$ (slope –piles)		$M_{o1}=M_{o2}$	• Same as E-E • $N_{pi}\neq 0$
P-EP				$M_{oi}=H_ie_{oi}$ at sliding level	• $w_{g1}=0$, $L_1<1.2L_{c1}+x_{p1}$; • Dependent on w_s e.g. Cases I and VII

Table 3 Input properties and parameters for E-E solutions

Piles			Soil	Sliding parameters				References	
$\frac{d}{t}$ (mm)	E_p (GPa)	$\frac{L_1}{L_2}$ (m)	$\frac{N_i}{s_{u1}/s_{u2}{}^a}$	$\frac{L_{c1}}{L_{c2}}$ (m)[b]	$\frac{k_1}{k_2}$ (MPa)	θ_o ($\times 10^{-3}$)	H (kN)		Cases
$\frac{790}{395}$	20	$\frac{7.5}{22.5}$	$\frac{-}{40/40}$	$\frac{7.7}{7.7}$	$\frac{8.0}{8.0}$	13	296	(Esu and D'Elia 1974)	I
$\frac{318.5}{6.9}$	210	$\frac{11.2}{12.8}$	$\frac{7.9/12.6}{-}$	$\frac{6.3}{5.6}$	$\frac{5.0}{8.0}$	26 [c]	150	Hataosi-2 (Cai and Ugai 2003)	II
$\frac{318.5}{6.9}$	210	$\frac{8.0}{9.0}$	$\frac{7.9/23.6}{-}$	$\frac{6.3}{4.9}$	$\frac{5.0}{15.0}$	4 [c]	70	Hataosi-3 (Cai and Ugai 2003)	III
$\frac{318.5}{6.9}$	210	$\frac{6.5}{7.5}$	$\frac{7.9/12.6}{-}$	$\frac{6.3}{5.6}$	$\frac{5.0}{8.0}$	-8 [c]	300	Kamimoku-4 (Cai and Ugai 2003)	IV
$\frac{318.5}{6.9}$	210	$\frac{4.0}{6.0}$	$\frac{7.9/12.6}{-}$	$\frac{6.3}{5.6}$	$\frac{5.0}{8.0}$	40 [c]	250	Kamimoku-6 (Cai and Ugai 2003)	V
$\frac{300}{60}$	20	$\frac{7.3}{5.7}$	$\frac{s_{u1}=30}{N_2=16.7}$ [d]	$\frac{3.2}{2.8}$	$\frac{6.0}{10.0}$	25 [c]	40	Katamachi-B (Cai and Ugai 2003)	VI
$\frac{1200}{600}$	20	$\frac{9.5}{13.0}$	$\frac{-}{30/30}$	$\frac{12.7}{12.7}$	$\frac{15}{15}$	9.0	500	Carrubba (Carrubba et al. 1989)	VII
$\frac{630}{315}$	28.45	$\frac{2.5}{10.0}$		$\frac{23.1}{23.1}$	$\frac{14.4}{28.8}$	0.5	60	Leung (2.5m)	VIII
$\frac{630}{315}$	28.45	$\frac{2.5}{10.0}$		$\frac{23.1}{23.1}$	$\frac{14.4}{28.8}$	0.5	85	Leung (3.5m)	VIII
$\frac{630}{315}$	28.45	$\frac{2.5}{10.0}$		$\frac{23.1}{23.1}$	$\frac{14.4}{28.8}$	0.5	100	Leung (4.5 m)	VIII

[a] s_{ui} (in kPa); [b] $G_{si} = k_i/3$ (k_i in Table 4) for estimating L_{ci} using the expression shown in Table 1; and [c] Calculated using measured pile deflection profiles (Cai and Ugai 2003); and [d] Sliding layer s_{u1} = 30 kPa.

Table 4 Input/output for P-EP solutions ($H = H_1 = -H_2$, $n_1 = 0$, and $n_2 = 1.0$)

Input data					Output			**Meas**	Case
$\frac{A_{L1}}{A_{L2}}$ (kN/m^{ni+1})	$\frac{k_1}{k_2}$ (MPa)	$\frac{w_s}{\xi}$ (mm)	e_{o2}[a] (m)	$\frac{x_s}{x_{p2}}$ (m)	$\frac{H(kN)}{\theta_o(\times 10^{-3})}$	$\frac{w_{g2}(mm)}{\lambda_2}$[b]	$\frac{\xi_{min}}{\xi_{max}}$	$\frac{M_{max\,2}(kNm)}{H_2(kN)}$	
$\frac{94.8}{52.0}$	$\frac{2.5}{8.0}$[c]	$\frac{110}{0.50}$	$\frac{0.78}{0.93}$	$\frac{2.78}{2.96}$	$\frac{316.2}{-12.3}$	$\frac{52.1}{0.273}$	$\frac{0.105}{9.556}$	$\frac{903}{310}$	I
$\frac{50.2}{80.4}$	$\frac{5.0}{8.0}$	$\frac{153}{0.05}$	$\frac{0.75}{0.77}$	$\frac{8.03}{1.73}$	$\frac{139.1}{-29.0}$	$\frac{61.0}{0.584}$	$\frac{0.05}{24.45}$	$\frac{165.2}{--}$	II
$\frac{50.2}{80.4}$	$\frac{5.0}{15.0}$	$\frac{27.0}{0.02}$	$\frac{0.35}{0.42}$	$\frac{6.45}{1.07}$	$\frac{69.6}{-8.47}$	$\frac{14.1}{0.683}$	$\frac{0.022}{44.85}$	$\frac{65.7}{--}$	III
$\frac{50.2}{80.4}$	$\frac{5.0}{8.0}$	$\frac{150}{0.8}$	$\frac{-0.25}{-0.24}$	$\frac{2.25}{1.56}$	$\frac{123.3}{-24.0}$	$\frac{49.0}{0.584}$	$\frac{0.081}{12.31}$	$\frac{123.2}{--}$	IV
$\frac{100.3}{140.5}$	$\frac{5.0}{8.0}$	$\frac{320}{5.67}$	$\frac{0.85}{0.91}$	$\frac{0.22}{1.79}$	$\frac{253.7}{-54.4}$	$\frac{116}{0.584}$	$\frac{0.176}{5.67}$	$\frac{290.3}{--}$	V[d]
$\frac{19.8}{39.6}$	$\frac{6.0}{10.0}$	$\frac{135}{0.3}$	$\frac{0.75}{0.91}$	$\frac{3.32}{1.82}$	$\frac{59.1}{-23.4}$	$\frac{42}{0.775}$	$\frac{0.09}{10.88}$	$\frac{69.0}{51.0}$	VI
$\frac{198}{79.2}$	$\frac{15}{15}$	$\frac{95.7}{0.3}$	$\frac{1.0}{0.87}$	$\frac{4.28}{3.05}$	$\frac{778.7}{-8.9}$	$\frac{49.2}{0.207}$	$\frac{0.09}{10.67}$	$\frac{2200}{1460}$	VII
$\frac{37.8}{18.9}$	$\frac{28.8}{28.8}$	$\frac{4.5}{0.0}$	$\frac{0.57}{0.60}$	$\frac{3.30}{1.83}$	$\frac{45.2}{-1.15}$	$\frac{3.1}{0.425}$	$\frac{0.05}{21.64}$	$\frac{60.0}{55.0}$	VIII
		$\frac{6.0}{0.00}$	$\frac{0.66}{0.69}$	$\frac{3.30}{2.06}$	$\frac{53.1}{-1.44}$	$\frac{4.1}{0.425}$	$\frac{0.06}{17.18}$	$\frac{75.0}{70.0}$	VIII
		$\frac{7.3}{0.0}$	$\frac{0.72}{0.76}$	$\frac{2.99}{2.23}$	$\frac{57.2}{-1.68}$	$\frac{4.8}{0.425}$	$\frac{0.07}{14.79}$	$\frac{82.0}{83.9}$	VIII

Note that [a]e_{o2}, denominator and numerator are calculated using Eq. (16) and (17), respectively. allowing a smooth transition of moment in sliding depth for the P-EP solution; [b] $\theta_o = -\theta_{g1} - \theta_{g2}$, with $\theta_o = -\theta_{g2}$ for rigid rotation with $L_1 < 1.2L_{c1} + x_{p1}$; [c] L_{c1}, L_{c2} = 10.35, and 8.0 m; [d] Use of positive θ_o rather than -0.008 (see Table 3); short piles, elastic analysis is only approximate.

APPENDIX RESPONSE PROFILES FOR E-E, P-EP SOLUTIONS

Determination of C_{5i} and C_{6i} for E-E Solution

The first, second, and third derivatives of Eq. (7) offer the rotation angle (slope), the bending moment, and the shear force, respectively.

$$\theta_{Bi}(z_i) = w'_{Bi}(z_i) = e^{-\alpha_i z_i}[(-\alpha_i C_{5i} + \beta_i C_{6i})\cos\beta_i z_i + (-\beta_i C_{5i} - \alpha_i C_{6i})\sin\beta_i z_i] \tag{25}$$

$$\begin{aligned} -M_{Bi}(z_i)/E_p I_p = w''_{Bi}(z_i) &= e^{-\alpha_i z_i}\{[(\alpha_i{}^2 - \beta_i{}^2)C_{5i} - 2\alpha_i\beta_i C_{6i}]\cos\beta_i z_i \\ &+ [2\alpha_i\beta_i C_{5i} + (\alpha_i{}^2 - \beta_i{}^2)C_{6i}]\sin\beta_i z_i\} \end{aligned} \tag{26}$$

$$\begin{aligned} -Q_{Bi}(z_i)/E_p I_p &= w'''_{Bi}(z_i) \\ &= e^{-\alpha_i z_i}[-\alpha_i(\alpha_i{}^2 - 3\beta_i{}^2)C_{5i} + \beta_i(3\alpha_i{}^2 - \beta_i{}^2)C_{6i}]\cos\beta_i z_i \\ &+ e^{-\alpha_i z_i}[-(3\alpha_i{}^2 - \beta_i{}^2)\beta_i C_{5i} - \alpha_i(\alpha_i{}^2 - 3\beta_i{}^2)C_{6i}]\sin\beta_i z_i \end{aligned} \tag{27}$$

At the sliding interface ($z_i = 0$), the following conditions are observed:
(1) With $\theta_{gi} = -\theta_i(z_i)$, $\theta_{gi} = -\alpha_i C_{5i} + \beta_i C_{6i}$ is noted from Eq. (27). The condition of $-\theta_{g1} + \theta_o = -\theta_{g2}$ can be rewritten as:

$$-(\alpha_1 C_{51} - \beta_1 C_{61}) + \theta_o = \alpha_2 C_{52} - \beta_2 C_{62} \tag{28}$$

(2) With $M_{oi}/E_pI_p = -w_{Bi}''(z_i)$, $M_{oi}/E_pI_p = (\alpha_i^2 - \beta_i^2)C_{5i} - 2\alpha_i\beta_i C_{6i}$ is obtained from Eq. (26). The expression of $M_{o1} = M_{o2}$ then becomes:

$$\alpha_1^2 C_{51} - 2\alpha_1\beta_1 C_{61} - \beta_1^2 C_{51} = \alpha_2^2 C_{52} - 2\alpha_2\beta_2 C_{62} - \beta_2^2 C_{52} \tag{29}$$

(3) With $H_i/E_pI_p = -w_{Bi}'''(z_i)$, and the shear force H, two expressions of $-E_pI_p w_{B1}'''(0) = H_1 = H$, and $-E_pI_p w_{B2}'''(0) = H_2 = -H$, can be written as:

$$(\alpha_1^3 C_{51} - 3\alpha_1^2\beta_1 C_{61} - 3\alpha_1\beta_1^2 C_{61} + \beta_1^3 C_{61})E_p I_p = H \tag{30}$$

$$(\alpha_2^3 C_{52} - 3\alpha_2^2\beta_2 C_{62} - 3\alpha_2\beta_2^2 C_{62} + \beta_2^3 C_{62})E_p I_p = H_2 = -H \tag{31}$$

The four equations (28), (29), (30), and (31) are resolved together to obtain the four factors that are combined to C_{5i} and C_{6i} of Eqs. (10) and (11). The depth of maximum bending moment z_{maxi} is obtained using $Q_{Bi}(z_{maxi}) = 0$.

$$z_{\max i} = \frac{1}{\beta_i}\tan^{-1}\left[\frac{-\alpha_i(\alpha_i^2 - 3\beta_i^2)C_{5i} + (3\alpha_i^2 - \beta_i^2)\beta_i C_{6i}}{(3\alpha_i^2 - \beta_i^2)\beta_i C_{5i} + \alpha_i(\alpha_i^2 - 3\beta_i^2)C_{6i}}\right] \tag{32}$$

Assuming $N_{pi} = 0$ (uncoupled), the C_{5i}, C_{6i}, and z_{maxi} etc reduce to previous solutions, as shown next.

Sliding Layer (E-E Uncoupled Solution)

Elastic response is stipulated for the sliding layer. Assuming $N_{pi} = 0$ ($\alpha_i = \beta_i = \lambda_i$), the constant C_{5i} and C_{5i} of Eqs. (10) and (11) are rewritten as

$$C_{5i} = (-1)^i \frac{H}{4} \frac{\lambda_i + \lambda_j}{\lambda_i^3 \lambda_j E_p I_p} + \frac{\theta_o}{2} \frac{\lambda_j}{\lambda_i(\lambda_i + \lambda_j)} \tag{33}$$

$$C_{6i} = (-1)^i \frac{H}{4} \frac{\lambda_j - \lambda_i}{\lambda_i^3 \lambda_j E_p I_p} - \frac{\theta_o}{2} \frac{\lambda_j}{\lambda_i(\lambda_i + \lambda_j)} \tag{34}$$

The C_{5i} and C_{5i} are essentially identical to those deduced previously (Cai and Ugai 2003). Accordingly, the elastic equations (25), (26) and (27) in Appendix I reduce to

$$\theta_{Bi}(z_i) = w'_{Bi}(z_i) = \lambda_i e^{-\lambda_i z_i}[(-C_{5i} + C_{6i})\cos\lambda_i z_i + (-C_{5i} - C_{6i})\sin\lambda_i z_i] \tag{35}$$

$$-M_{Bi}(z_i)/E_p I_p = w''_{Bi}(z_i) = 2\lambda_i^2 e^{-\lambda_i z_i}\{-C_{6i}\cos\lambda_i z_i + C_{5i}\sin\lambda_i z_i\} \tag{36}$$

$$\begin{aligned} -Q_{Bi}(z_i)/E_p I_p &= w'''_{Bi}(z_i) \\ &= 2\lambda_i^3 e^{-\lambda_i z_i}\{[C_{5i} + C_{6i}]\cos\lambda_i z_i - [C_{5i} - C_{6i}]\sin\lambda_i z_i\} \end{aligned} \tag{37}$$

The z_i is measured from sliding interface. Finally, the depth of M_{maxi} is simplified to

$$z_{max\,i} = \frac{1}{\beta_i}\tan^{-1}\left[\frac{C_{5i} + C_{6i}}{C_{5i} - C_{6i}}\right] \tag{38}$$

Stable Layer (EP Solution)

The elastic-plastic solutions are used to gain the response profiles in stable layer. In plastic state, the force $Q_{A2}(x_2)$, moment $M_{A2}(x_2)$, deflection $w_{A2}(x_2)$ and rotation $\theta_{A2}(x_2)$ at depth x_2 ($\leq x_{p2}$) are as follows:

$$\begin{aligned} w_{A2}(x_2) = \frac{A_{L2}}{E_p I_p}\{&-F(4,x_2) + F(4,0) + F(3,0) + [F(2,0) + \frac{M_{o2}}{A_{L2}}]\frac{x_2^2}{2} \\ &+ [F(1,0) + \frac{H_i}{A_{L2}}]\frac{x_2^3}{6}\} + \theta_{g2}x_2 + w_{g2} \end{aligned} \tag{39}$$

$$\theta_{A2}(x_2)=\frac{A_{L2}}{E_pI_p}\{-F(3,x_2)+F(3,0)+[F(2,0)+\frac{M_{o2}}{A_{L2}}]x_2+[F(1,0)+\frac{H_2}{A_{L2}}]\frac{x_2^2}{2}\}+\theta_{g2} \quad (40)$$

$$-M_{A2}(x_2)=\{-F(2,x_2)+F(2,0)+[F(1,0)+\frac{H_2}{A_{L2}}]x_2\}A_{L2}+M_{o2} \quad (41)$$

$$-Q_{A2}(x_2)=A_{L2}[-F(1,x_2)+F(1,0)+\frac{H_2}{A_{L2}}] \quad (42)$$

In elastic zone with subscript 'B' ($x_2 > x_{p2}$), they are given by the following

$$\begin{aligned} w_{B2}(z_2)=\frac{e^{-\alpha_2 z_2}E_pI_p}{k_2}\{&[2\alpha_2 w'''_{P2}+(3\alpha_2^2-\beta_2^2)w''_{P2}]\cos\beta_2 z_2 \\ &+[(\alpha_2^2-\beta_2^2)w'''_{P2}+\alpha_2(\alpha_2^2-3\beta_2^2)w''_{P2}]\frac{\sin\beta_2 z_2}{\beta_2}\} \end{aligned} \quad (43)$$

$$-\theta_{B2}(z_2)=\frac{e^{-\alpha_2 z_2}}{2\lambda_2^2}\{(w'''_{P2}+2\alpha_2 w''_{P2})\cos\beta_2 z_2+[\alpha_2 w'''_{P2}+(\alpha_2^2-\beta_{2i}^2)w''_{P2}]\frac{\sin\beta_2 z_2}{\beta_2}\} \quad (44)$$

$$-M_{B2}(z_2)=E_pI_pe^{-\alpha_2 z_2}[w''_{P2}\cos\beta_2 z_2+(w'''_{P2}+\alpha_2 w''_{P2})\frac{\sin\beta_2 z_2}{\beta_2}] \quad (45)$$

$$-Q_{B2}(z_2)=E_pI_pe^{-\alpha_2 z_2}[w'''_{P2}\cos\beta_2 z_2-(\alpha_2 w'''_{P2}+2\lambda_2^2 w''_{P2})\frac{\sin\beta_2 z_2}{\beta_2}] \quad (46)$$

$$z_{\max 2}=\frac{1}{\beta_2}\tan^{-1}(\beta_2 w'''_{P2}/[\alpha_2 w'''_{P2}+2\lambda_2^2 w''_{P2}]) \quad (47)$$

where

$$F(m,x_2)=\frac{(x_2+\alpha_{o2})^{n_2+m}}{(n_2+m)...(n_2+1)}\ (\text{m = 1-4}) \quad (48)$$

$$w'''_{P2}=\frac{A_{L2}}{E_pI_p}[-F(1,x_{p2})+F(1,0)+\frac{H_2}{A_{L2}}] \quad (49)$$

$$w''_{P2}=\frac{A_{L2}}{E_pI_p}[-F(2,x_{p2})+F(2,0)+F(1,0)x_{p2}+\frac{H_2x_{p2}}{A_{L2}}+\frac{M_{o2}}{A_{L2}}] \quad (50)$$

where w''_{p2} and w'''_{p2} are values of 2rd and 3th derivatives of $w_2(x_2)$ with respect to z_2 (= x_2-x_{p2}). At $n_2 = 1$, the following simple expressions are noted

$$w''_{P2}=\frac{A_{L2}}{E_pI_p\lambda_2^3}\frac{x_{p2}^2}{6}\frac{2x_{p2}+3}{1+x_{p2}} \quad (51)$$

$$w'''_{P2} = \frac{A_{L2}}{E_p I_p \lambda_2^2} \frac{-x_{p2}}{6} \frac{2x_{p2}^2 - 3}{1 + x_{p2}} \tag{52}$$

$$z_{\max 2} = \frac{-1}{\beta_2} \tan^{-1}\left[\frac{\beta_2 (2x_{p2}^2 - 3)}{\alpha_2 (2x_{p2}^2 + 3) + 6\lambda_2 x_{p2}}\right] \tag{53}$$

Given $N_{p2} = 0$ (i.e. $\alpha_2 = \beta_2 = \lambda_2$), Eqs. (43) – (47), (53), reduce to those deduced using a Winkler model. The maximum bending moment M_{max2} and its depth x_{max2} depend on the normalised depth $\bar{x}_{\max 2}$ (= $x_{max2}\lambda_2$).

$$\bar{x}_{\max 2} = a\tan\{1/\{1 + 2[\frac{-\bar{x}_{p2}^{n_2+2}}{(n_2+1)(n_2+2)} + (\bar{x}_{p2} + \bar{e}_{o2})\overline{H}_i]/(\frac{-\bar{x}_{p2}^{n_2+1}}{n_2+1} + \overline{H}_2)\}\} \tag{54}$$

The M_{max2} lies in plastic zone if $\bar{x}_{\max 2} < 0$, otherwise in elastic zone. It is calculated using one of the following expressions.

$$-M_{\max 2} = \frac{A_{L2}}{\lambda_2^{n_2+2}}\{\frac{1}{n_2+2}[(n_2+1)\overline{H}_2]^{(n_2+2)/(n_2+1)} + \overline{H}_2\bar{e}_{o2}\} \quad (x_{max2} < 0) \tag{55}$$

$$\begin{aligned} -M_{\max 2} = \frac{A_{L2}}{\lambda_2^{n_2+2}} e^{-\bar{x}_{\max 2}}\{&[\frac{-\bar{x}_{p2}^{n_2+2}}{(n_2+1)(n_2+2)} + (\bar{x}_{p2} + \bar{e}_{o2})\overline{H}_2]\cos(\bar{x}_{\max 2}) \\ &+ [\frac{-\bar{x}_{p2}^{n_2+1}}{n_2+1} + \overline{H}_i + \frac{-\bar{x}_{p2}^{n_2+2}}{(n_2+1)(n_2+2)} + (\bar{x}_{p2} + \bar{e}_{o2})\overline{H}_2]\sin(\bar{x}_{\max 2})\} \end{aligned} \quad (x_{max2} \geq 0) \tag{56}$$

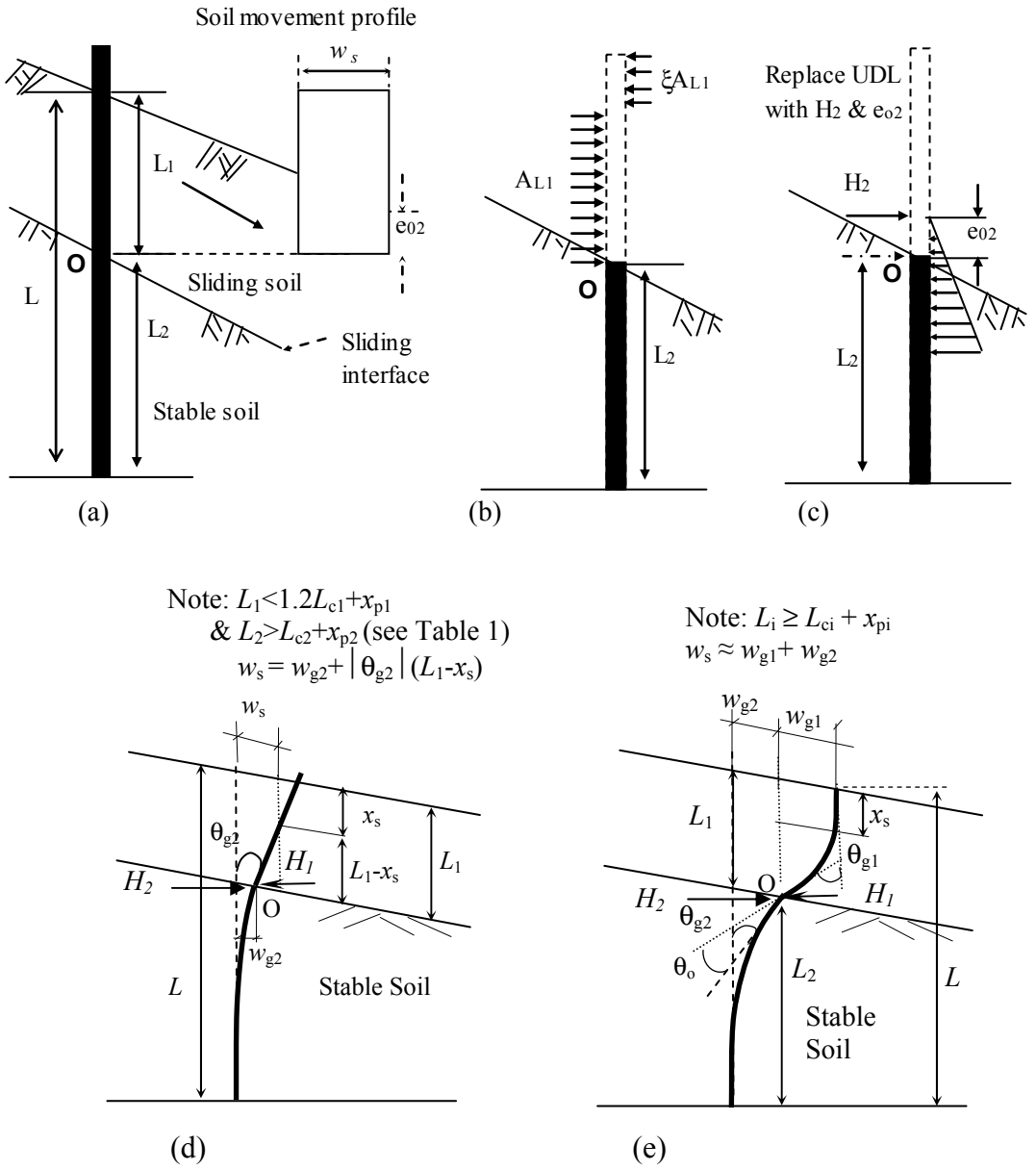

Fig.1. An equivalent load model for a passive pile: (a) The problem, (b) The imaginary pile, (c) Equivalent load H_2 and eccentricity e_{o2}; (d) Normal sliding, and (e) Deep sliding

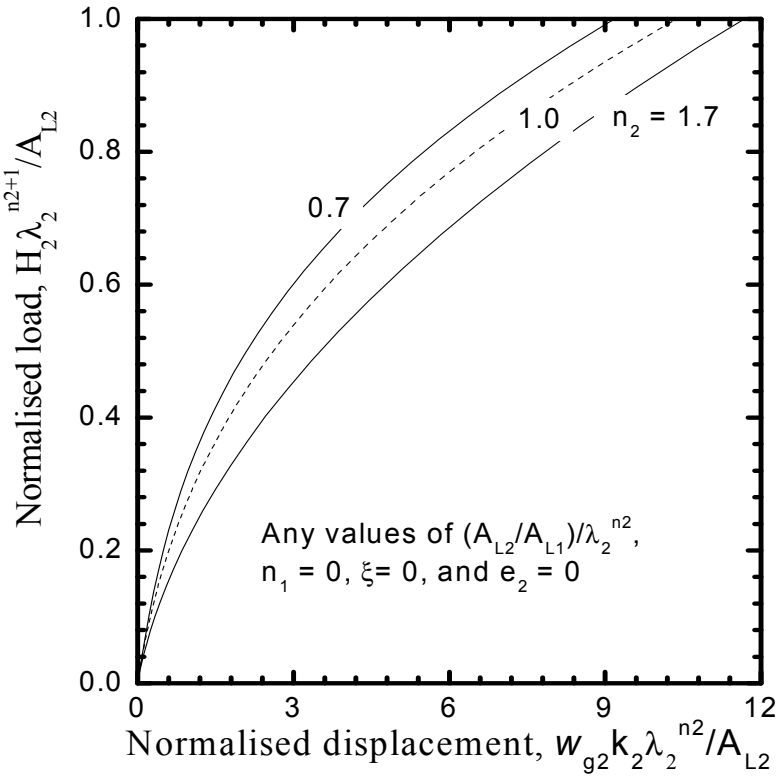

Fig.2. Response of piles in normal sliding mode

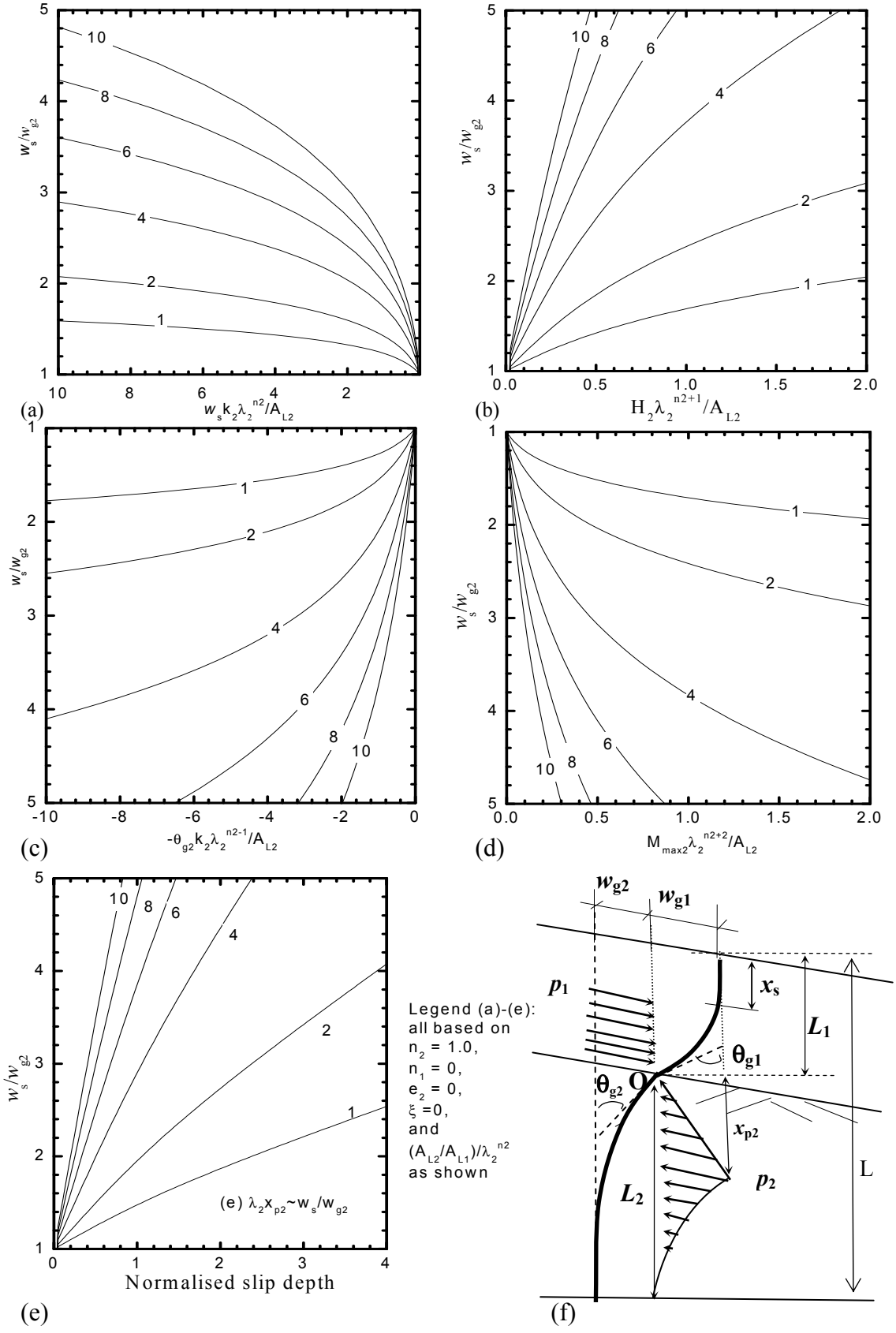

Fig.3. Normalised pile response in stable layer owing to soil movement w_s ($n_2 = 1$, $n_1 = 0$, $e_{o2} = 0$, $\xi = 0$): (a) Soil movement, (b) Load, (c) Slope, (d) Maximum moment, (e) Slip depth, and (f) Schematic stress distributions

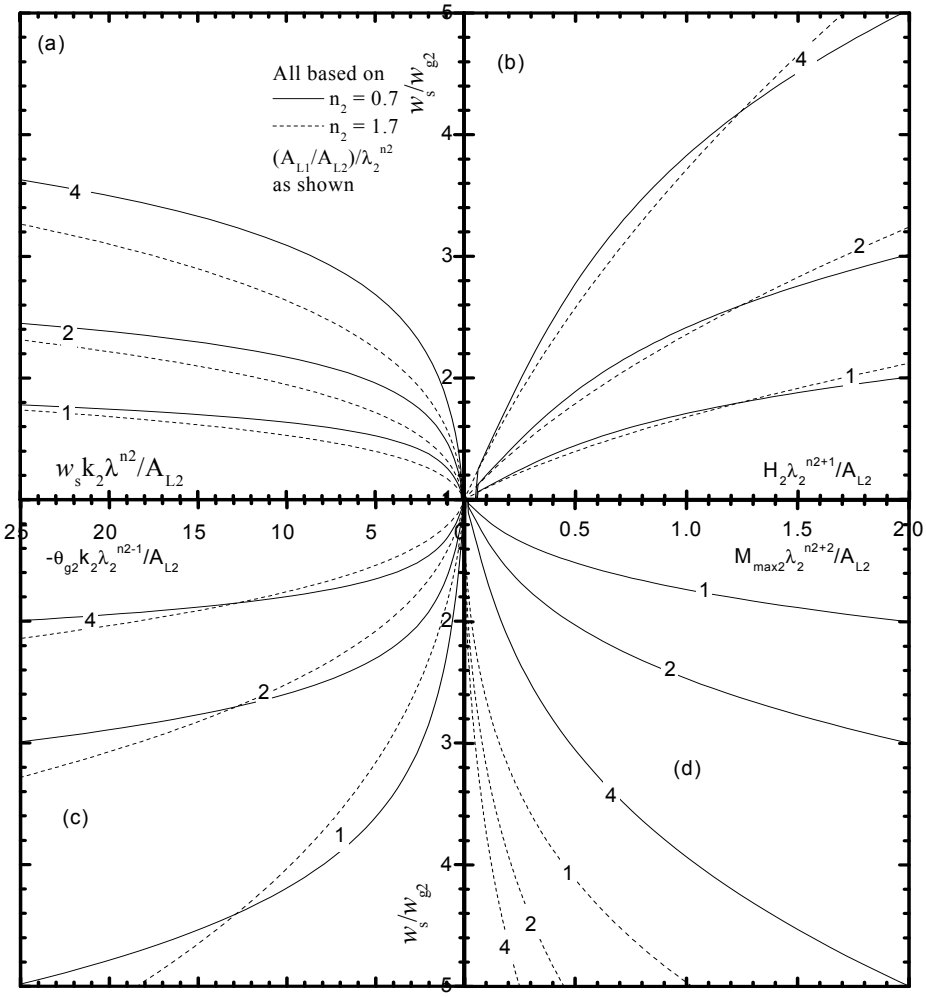

Fig.4. Effect of soil profile (n_2 = 0.7~1.7, n_1 = 0, e_{o2} = 0, ξ = 0) on normalized pile response in stable layer: (a) Soil movement, (b) Load, (c) Slope, and (d) Maximum moment

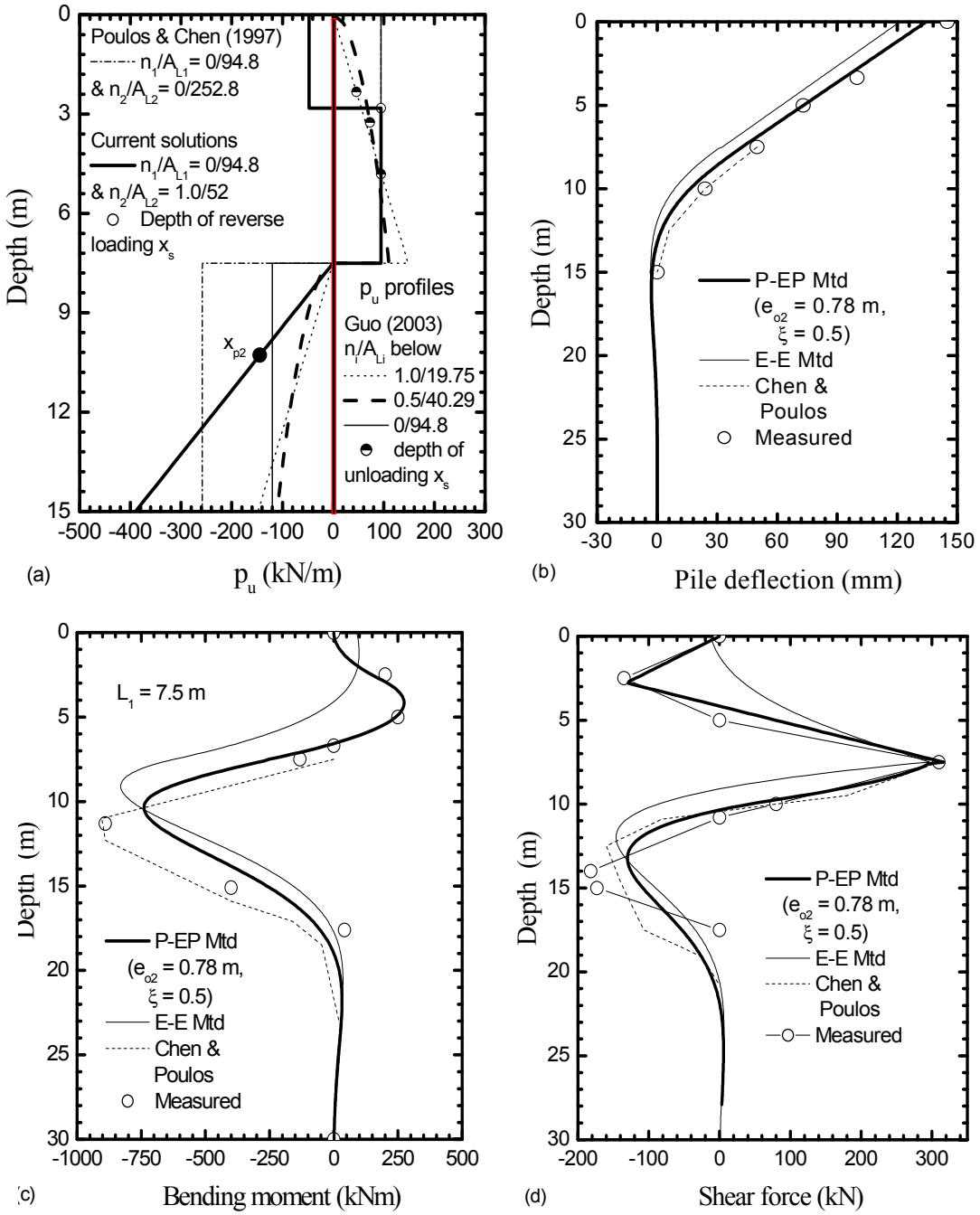

Fig.5. Predicted (using $\theta_o = -\theta_{g2}$) vs. measured (Esu and D'Elia 1974) responses (Case I): (a) bending moment, (b) pile deflection, and (c) shear force

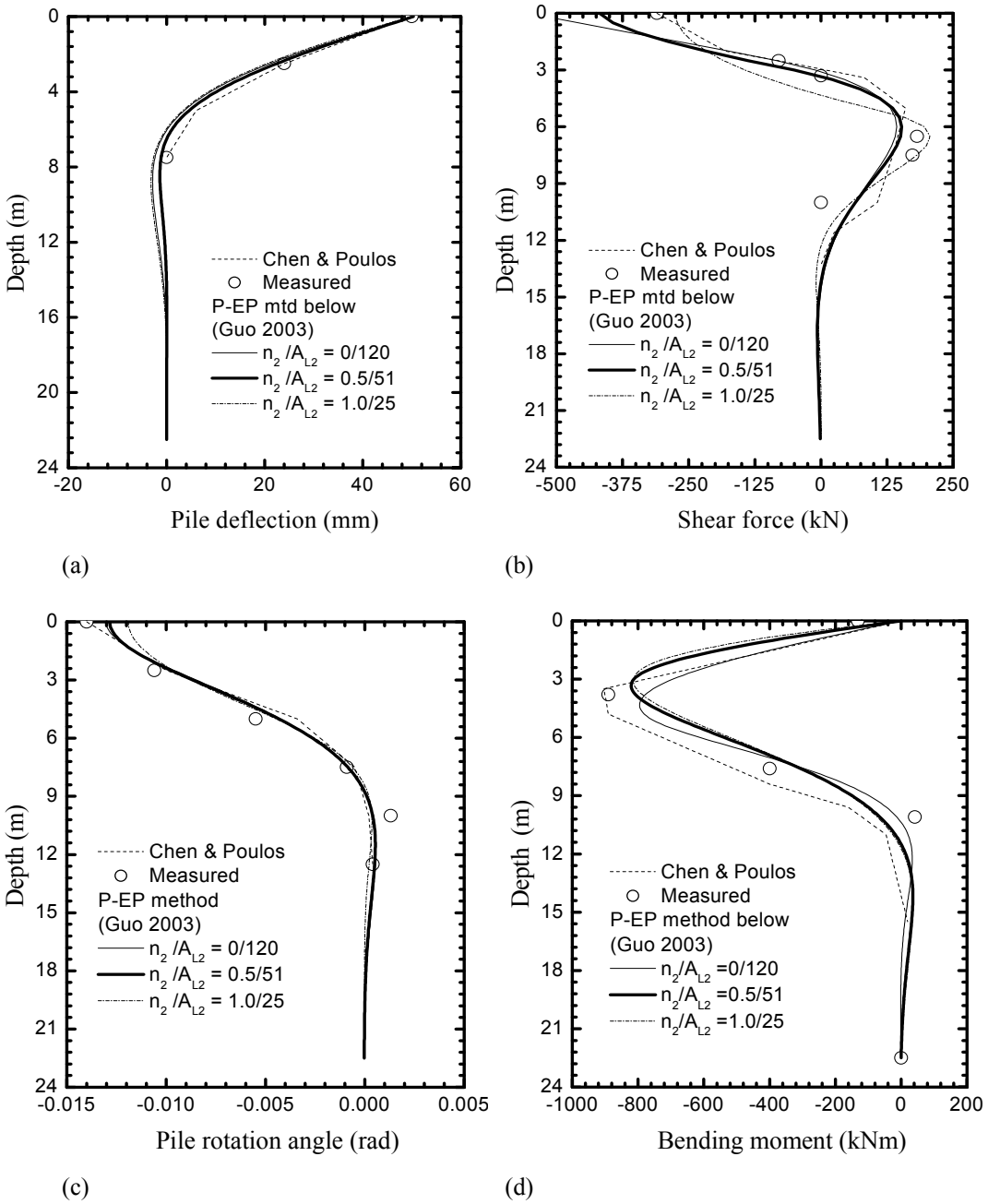

Fig.6. Effect of n_2 and A_{L2} (n_2/A_{L2} = 0./120; = 0.5/51.0, and 1.0/ 25.0; A_{L2} in kPa) on the predicted pile response (Case I) in stable layer: (a) pile deflection, (b) shear force, (c) pile rotation, and (d) bending moment

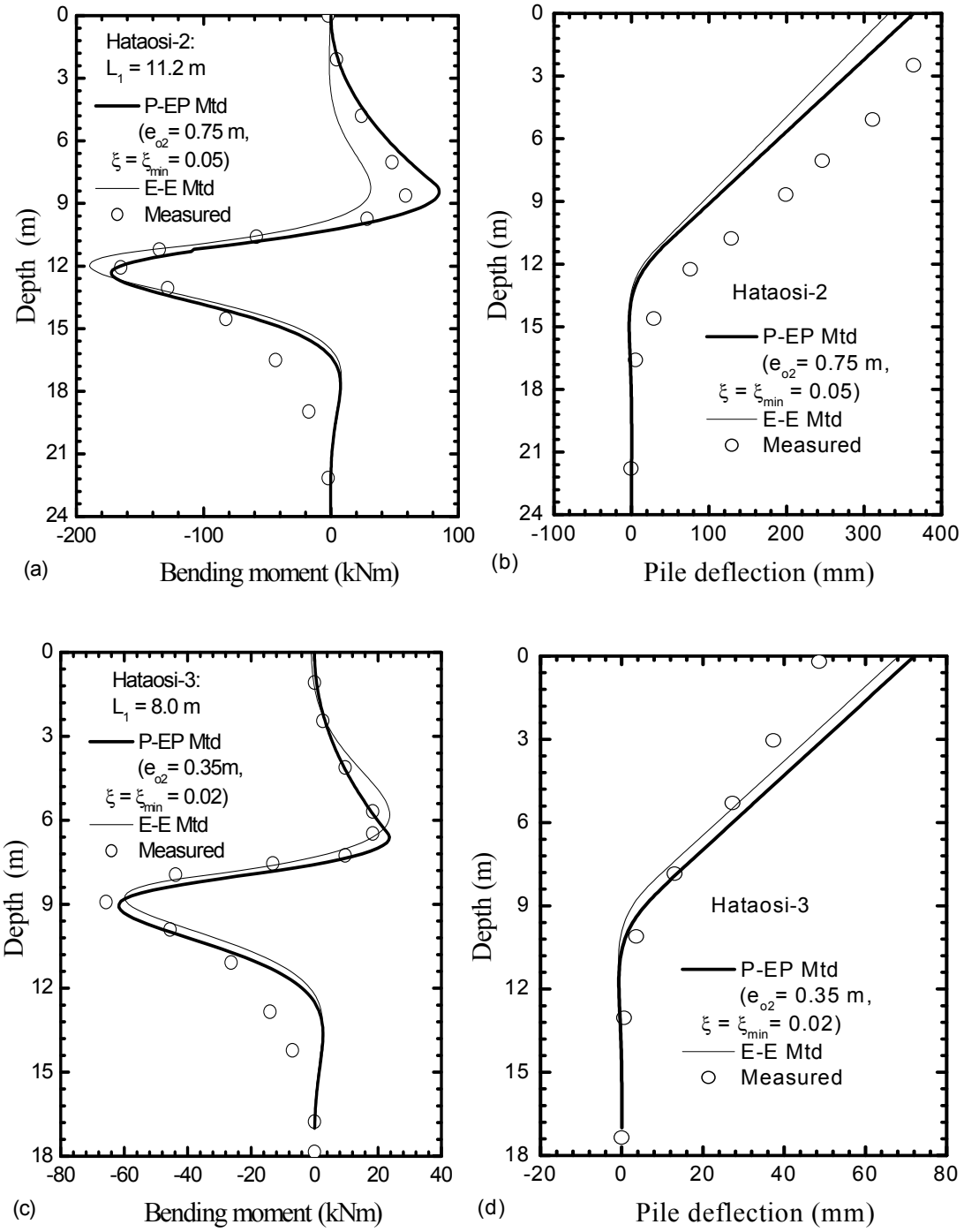

Fig.7. Predicted versus measured pile responses: (a) moment and (b) deflection for Case II, (c) moment and (d) deflection for Case III

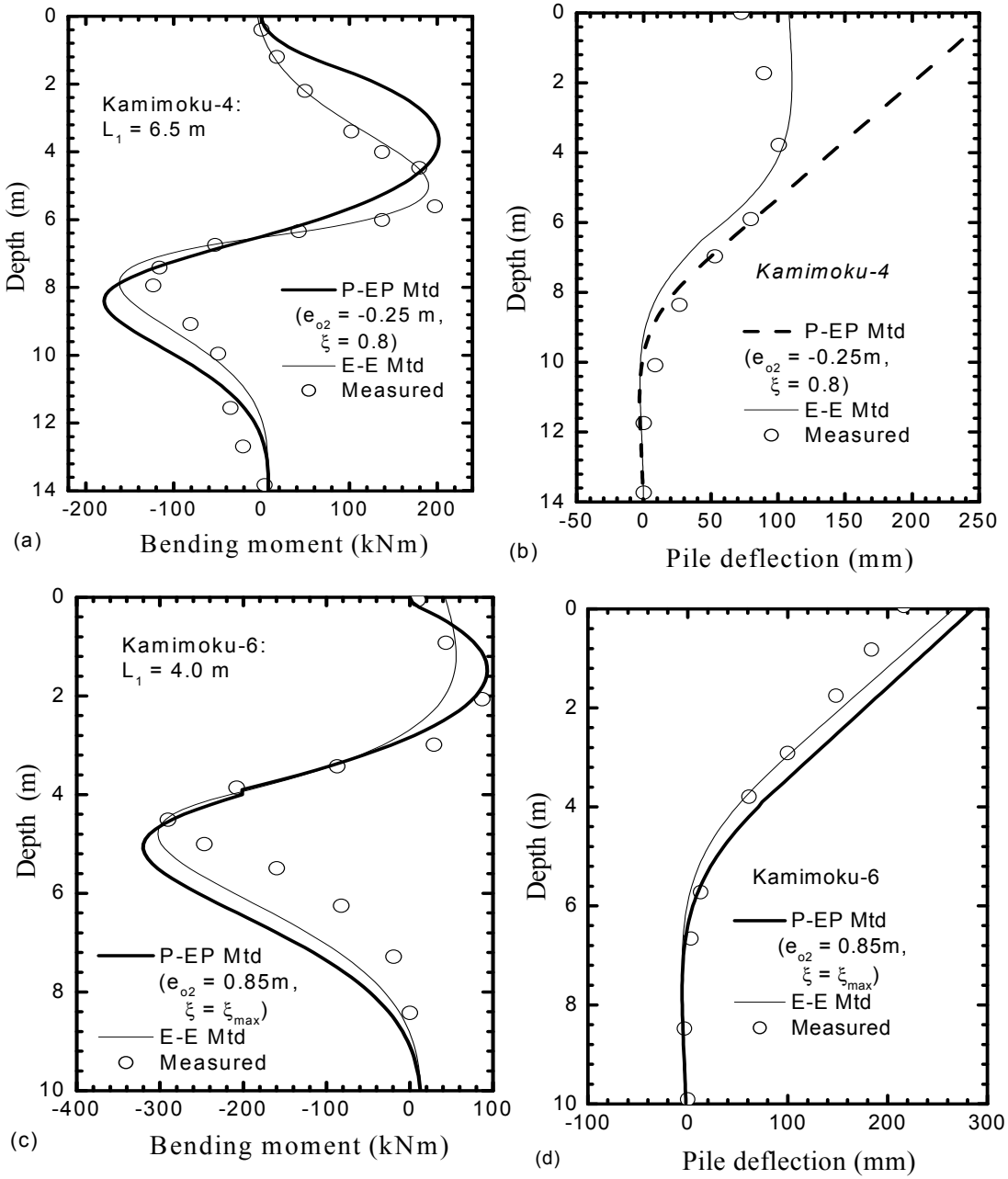

Fig.8. Predicted versus measured pile responses: (a) moment and (b) deflection for Case IV, (c) moment and (d) deflection for Case V

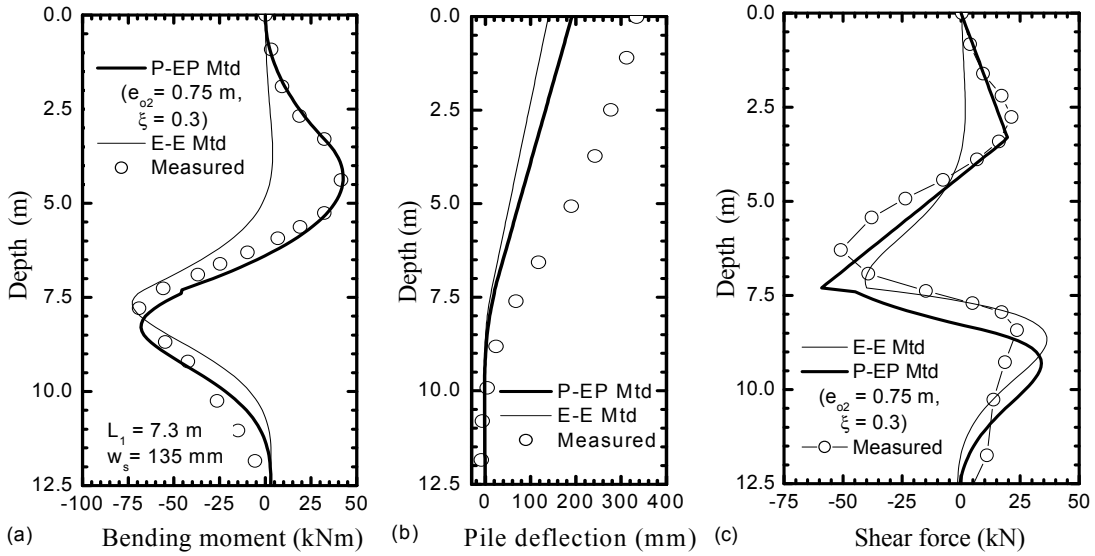

Fig.9. Predicted (using $\theta_o = -\theta_{g2}$) vs. measured responses (Case VI): (a) bending moment, (b) deflection and (c) shear force at w_s = 135 mm

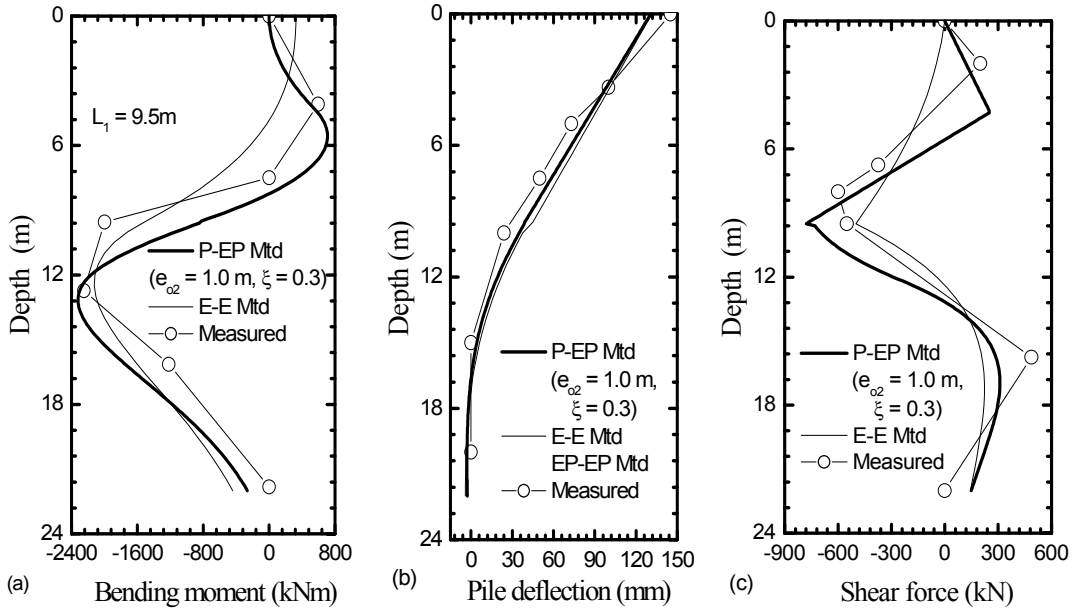

Fig. 10. Predicted (using $\theta_o = -\theta_{g2}$) versus measured (Carrubba et al. 1989) pile responses (Case VII): (a) bending moment, (b) pile deflection, and (c) shear force

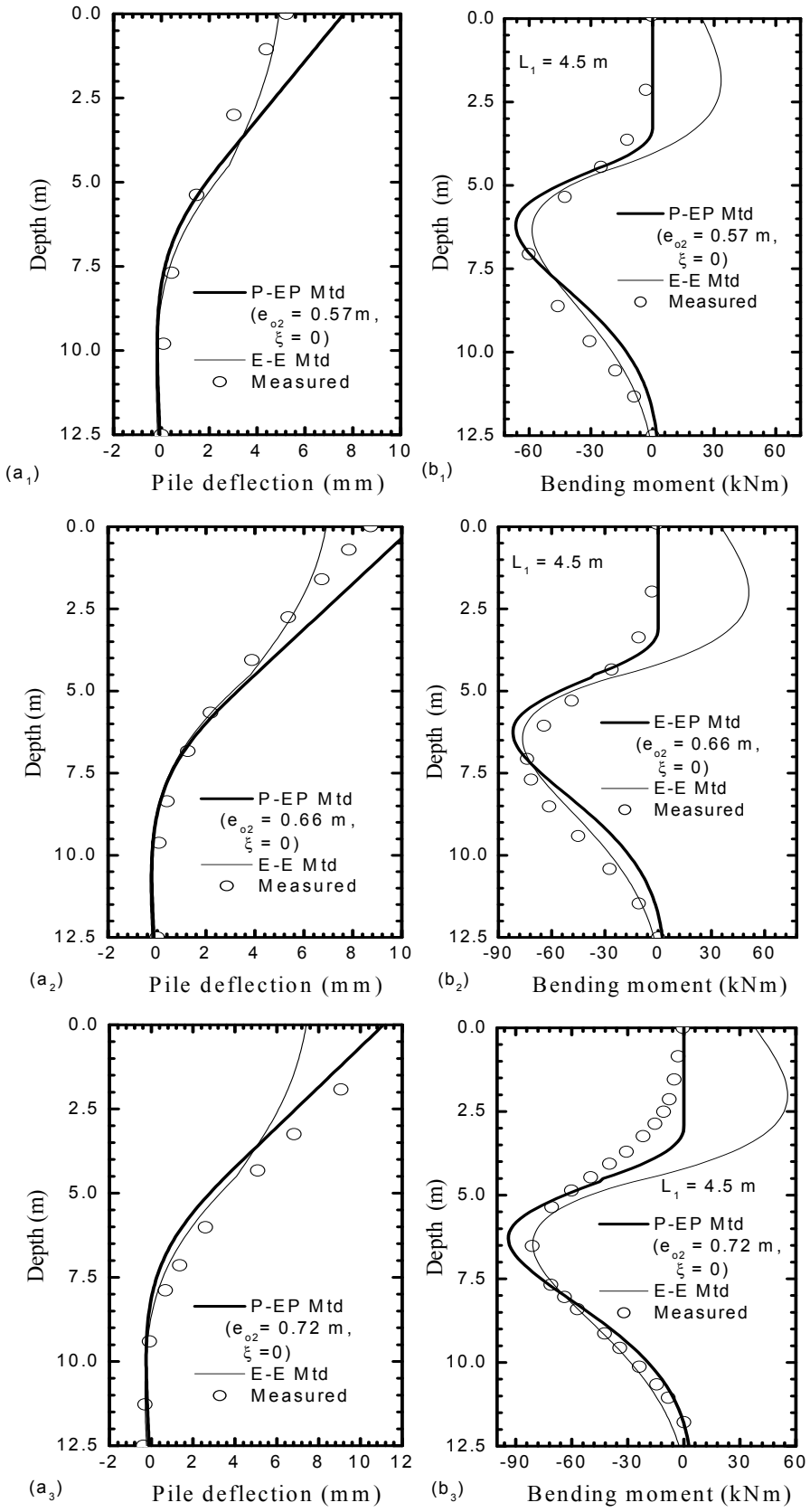

Fig. 11 Predicted versus measured pile response during excavation (Leung et al. 2000) (Case VIII): (a_1) deflection and (b_1) bending moment at 2.5 m; (a_2) deflection and (b_2) bending moment at 3.5 m; and (a_3) deflection and (b_3) bending moment at 4.5 m

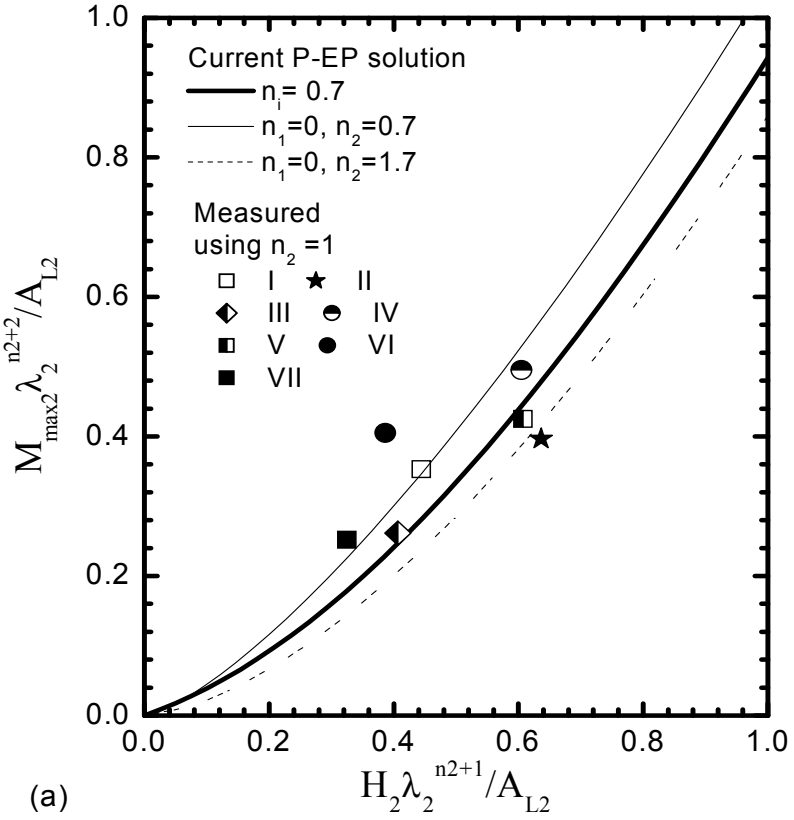

(a)

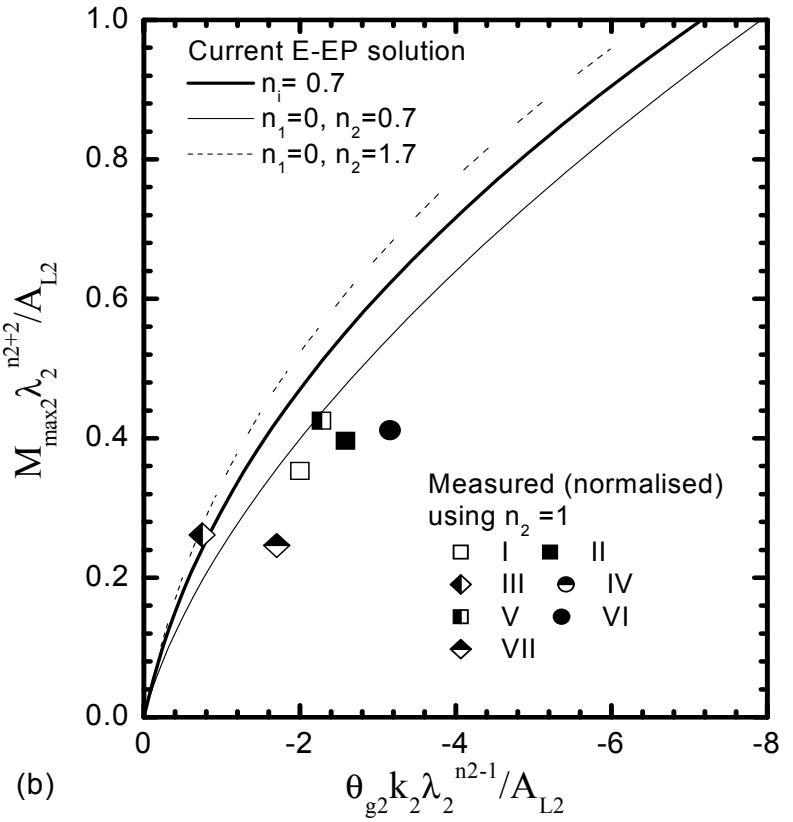

(b)

Fig.12 Predicted versus measured pile responses for all cases: (a) Normalized load versus moment, and (b) Normalized rotation angle versus moment